INTEGRATION AND PERFORMANCE ANALYSIS OF A SOLAR-DRIVEN COMBINED COOLING, HEATING, AND POWER SYSTEM: A CASE STUDY IN LIBYA

2025
MASTER THESIS
MECHANICAL ENGINEERING

Salah Khalefa ABORAGIGA

Thesis Advisor
Assist. Prof. Dr. Abdulrazzak Ahmet Saleh AKROOT

INTEGRATION AND PERFORMANCE ANALYSIS OF A SOLAR-DRIVEN COMBINED COOLING, HEATING, AND POWER SYSTEM: A CASE STUDY IN LIBYA

Salah Khalefa ABORAGIGA

Thesis Advisor
Assist. Prof. Dr. Abdulrazzak Ahmet Saleh AKROOT

T.C.
Karabuk University
Institute of Graduate Programs
Department of Mechanical Engineering
Prepared as
Master Thesis

KARABUK
May 2025

I certify that, in my opinion the presented thesis that has been submitted by Salah Khalefa ABORAGIGA titled “INTEGRATION AND PERFORMANCE ANALYSIS OF A SOLAR-DRIVEN COMBINED COOLING, HEATING, AND POWER SYSTEM: A CASE STUDY IN LIBYA” is fully adequate in scope and quality as a thesis for the degree of Master of Science

Assist. Prof. Dr. Abdulrazzak Ahmed Saleh AKROOT .....
Thesis Advisor, Department of Mechanical Engineering

This thesis is accepted by the examining committee with a unanimous vote in the Dept of Mechanical Engineering as Master of Science thesis. 30/05/2025

Examining Committee Members (Institutions) Signature

Chairman : Assist.Prof.Dr. Abdulrazzak A. Saleh AKROOT (KBU) .....

Member : Prof. Dr. Emrah DENİZ (KBU) .....

Member : Assist. Prof. Dr. Yousif Hashim HUSSEIN (Kerkük Uni.).....

The degree of Master of Science by the thesis that has been submitted was approved by the Administrative Board of the Institute of Graduate Programs, Karabuk University.

Assoc. Prof. Dr. Zeynep ÖZCAN .....
Director of the Institute of Graduate Programs

"I declare that all the information within this thesis has been gathered and presented in accordance with academic regulations and ethical principles, and I have cited all those which do not originate in this work according to the requirements of these regulations and principles."

Salah Khalefa ABORAGIGA

ABSTRACT

Master Thesis

INTEGRATION AND PERFORMANCE ANALYSIS OF A SOLAR-DRIVEN COMBINED COOLING, HEATING, AND POWER SYSTEM: A CASE STUDY IN LIBYA

Salah Khalefa ABORAGIGA

Karabük University
Institute of Graduate Programs
Department of Mechanical Engineering

Thesis Advisor:
Assist. Prof. Dr. Abdulrazzak Ahmet Saleh AKROOT
May 2025, 90 pages

The increasing demand for sustainable and efficient energy systems, particularly in regions with abundant solar resources such as Libya, has underscored the need for innovative solutions to address energy shortages, reduce environmental impacts, and enhance energy security. This study proposes and evaluates a novel solar-powered Combined Cooling, Heating, and Power (CCHP) system, specifically tailored for Libya's climatic and energy conditions. The importance of this research stems from Libya's heavy reliance on fossil fuels for energy production, its underutilized solar potential, and the critical need for diversified, resilient energy systems capable of delivering continuous power, heating, and cooling simultaneously.

The originality of the present study lies in the integration of a regenerative Brayton cycle, powered exclusively by concentrated solar energy, with an absorption cooling subsystem and thermal recovery unit, forming a fully solar-driven CCHP configuration. Unlike previous works that primarily address conventional CCHP systems or hybrid renewable integrations, this research uniquely models the combined thermodynamic behavior of a solar-powered regenerative Brayton-ARS system under the real-world climatic conditions of Tripoli, Libya. A further distinctive contribution is the detailed exergy analysis performed at the component level, highlighting key areas of irreversibility and guiding potential system improvements.

The main findings of the simulation and performance analysis reveal that the system achieves a net electrical output of approximately 11,987 kW, along with a heating load of 5,523 kW and a cooling load of 6,816 kW. The overall CCHP energy efficiency reaches 83.67%, while the exergy efficiency stands at 45.59%, demonstrating effective energy utilization across all three energy forms. The electrical energy and exergy efficiencies are recorded at 41.23% and 43.42%, respectively, indicating the system's strong capability to convert solar energy into high-quality electrical power. The coefficient of performance (COP) of the absorption refrigeration system is approximately 0.81, which is typical for single-effect LiBr-water absorption systems.

A detailed exergy destruction analysis showed that the solar receiver is the major contributor to system irreversibility, accounting for 45.33% of total exergy destruction. Other significant losses occur in the generator and heater components. The gas turbine and receiver exhibited high exergy efficiencies of 95.67% and 88.42%, respectively, highlighting their robust thermodynamic performance. Sensitivity analysis demonstrated that increasing the Brayton cycle pressure ratio improves net power output while slightly decreasing the heating and cooling loads.

Overall, the results confirm that the proposed system offers a highly efficient, sustainable, and regionally adapted solution for addressing Libya's pressing energy challenges. The findings provide valuable insights for future large-scale solar CCHP deployments in similar arid and high-solar-potential regions.

Keywords **:** Combined cooling, Heating, and power (CCHP), Thermodynamic modeling, Renewable energy integration, Libya

Science Code : 91436

ÖZET

Yüksek Lisans Tezi

GÜNEŞ ENERJİLİ KOMBİNE SOĞUTMA, ISITMA VE GÜÇ SİSTEMİNİN ENTEGRASYONU VE PERFORMANS ANALİZİ: LİBYA'DA BİR ALAN ÇALIŞMASI

Salah Khalefa ABORAGIGA

Karabük Üniversitesi
Lisansüstü Eğitim Enstitüsü
Makina Mühendisliği Anabilim Dalı

Tez Danışmanı:
Dr. Öğr. Üyesi Abdulrazzak Ahmet Saleh AKROOT
Mayıs 2025, 90 sayfa

Özellikle Libya gibi bol güneş enerjisi kaynaklarına sahip bölgelerde sürdürülebilir ve verimli enerji sistemlerine yönelik artan talep, enerji kıtlığını gidermek, çevresel etkileri azaltmak ve enerji güvenliğini artırmak için yenilikçi çözümlere duyulan ihtiyacın altını çizmiştir. Bu çalışma, Libya'nın iklim ve enerji koşullarına özel olarak uyarlanmış, güneş enerjisiyle çalışan yeni bir Kombine Soğutma, Isıtma ve Güç (CCHP) sistemi önermekte ve değerlendirmektedir. Bu araştırmanın önemi, Libya'nın enerji üretimi için fosil yakıtlara olan aşırı bağımlılığından, yeterince kullanılmayan güneş enerjisi potansiyelinden ve aynı anda sürekli güç, ısıtma ve soğutma sağlayabilen çeşitlendirilmiş, esnek enerji sistemlerine olan kritik ihtiyaçtan kaynaklanmaktadır.

Bu çalışmanın özgünlüğü, yalnızca yoğunlaştırılmış güneş enerjisiyle çalışan rejeneratif bir Brayton çevriminin, bir soğurmalı soğutma alt sistemi ve termal geri kazanım ünitesi ile entegre edilerek tamamen güneş enerjisiyle çalışan bir CCHP konfigürasyonu oluşturmasında yatmaktadır. Öncelikle geleneksel CCHP sistemlerini veya hibrit yenilenebilir entegrasyonları ele alan önceki çalışmaların aksine, bu araştırma, Libya'nın Trablus kentinin gerçek iklim koşulları altında güneş enerjisiyle çalışan rejeneratif Brayton-ARS sisteminin birleşik termodinamik davranışını benzersiz bir şekilde modellemektedir. Diğer bir ayırt edici katkı, bileşen düzeyinde gerçekleştirilen ayrıntılı ekserji analizidir, tersinmezliğin kilit alanlarını vurgulamakta ve potansiyel sistem iyileştirmelerine rehberlik etmektedir.

Simülasyon ve performans analizinin ana bulguları, sistemin 5.523 kW ısıtma yükü ve 6.816 kW soğutma yükü ile birlikte yaklaşık 11.987 kW net elektrik çıkışı elde ettiğini ortaya koymaktadır. Genel CCHP enerji verimliliği %83,67'ye ulaşırken, ekserji verimliliği %45,59'dur ve üç enerji formunda da etkin enerji kullanımını göstermektedir. Elektrik enerjisi ve ekserji verimlilikleri sırasıyla %41,23 ve %43,42 olarak kaydedilmiştir, bu da sistemin güneş enerjisini yüksek kaliteli elektrik enerjisine dönüştürme konusundaki güçlü kabiliyetini göstermektedir. Absorpsiyonlu soğutma sisteminin performans katsayısı (COP) yaklaşık 0,81'dir ve bu değer tek etkili LiBr-su absorpsiyon sistemleri için tipiktir.

Detaylı bir ekserji yıkım analizi, güneş enerjisi alıcısının toplam ekserji yıkımının %45,33'ünü oluşturarak sistemin tersinmezliğine en büyük katkıyı yaptığını göstermiştir. Diğer önemli kayıplar jeneratör ve ısıtıcı bileşenlerinde meydana gelmektedir. Gaz türbini ve alıcı, sırasıyla %95,67 ve %88,42 gibi yüksek ekserji verimlilikleri sergileyerek sağlam termodinamik performanslarını vurgulamıştır. Hassasiyet analizi, Brayton çevrimi basınç oranının artırılmasının net güç çıkışını iyileştirirken ısıtma ve soğutma yüklerini hafifçe azalttığını göstermiştir.

Genel olarak sonuçlar, önerilen sistemin Libya'nın acil enerji sorunlarını ele almak için son derece verimli, sürdürülebilir ve bölgesel olarak uyarlanmış bir çözüm sunduğunu doğrulamaktadır. Bulgular, benzer kurak ve yüksek güneş potansiyeli olan bölgelerde gelecekteki büyük ölçekli güneş CCHP dağıtımları için değerli bilgiler sağlamaktadır.

Anahtar Sözcükler : Kombine soğutma, Isıtma ve güç (CCHP), Termodinamik modelleme, Yenilenebilir enerji entegrasyonu, Libya.

Bilim Kodu **:** 91436

ACKNOWLEDGMENT

Praise be to God, who has given me the strength and perseverance to complete this research, and I ask God to benefit students through it.

I would like to express my sincere gratitude and deep appreciation to my supervisor, Assist. Prof. Dr. Abdulrazak Ahmed Saleh AKROOT.

I extend my sincere thanks to my colleagues and friends at Karabuk University for their cooperation, support, and camaraderie. The academic discussions and moments of shared learning have greatly enriched my experience and contributed to my personal and professional growth.

I also extend my sincere appreciation to the administrative staff at Karabuk University—the Graduate Programs Institute and the Department of Mechanical Engineering—for their professionalism and assistance in ensuring smooth administrative procedures throughout my graduate studies.

To my beloved family, I owe everything. Thank you for instilling in me the values of perseverance and a passion for learning, which have continued throughout my life. To my entire family,

This journey has been challenging and life-changing. I reflect on this chapter with deep appreciation for everyone who has supported me. The knowledge I gained and the relationships I built will remain a lasting legacy of this academic endeavor.

CONTENTS

Page

Page

Page

LIST OF FIGURES

Page

Page

LIST OF TABLES

Page

SYMBOLS AND ABBREVIATIONS INDEX

SYMBOL

A_{coll}	: collector area (cm2)
COP	: coefficient of performance
DNI	: direct normal Irradiations (W/m2)
$\dot{E}$	: energy (kW)
$\dot{EX}$	: exergy flows (kW)
h	: specific enthalpy (kJ/kg)
$\dot{m}$	: mass flow rate (kg/s)
P	: pressure (kPa)
$\dot{Q}$	: heat transfer (kW)
s	: specific entropy (kJ/kg. K)
T	: temperature (°C)
U	: overall heat transfer coefficient (W/m2.K)
$\dot{W}$	: work done (kW)

GREEK SYMBOLS

ŋ	: efficiency (%)
ψ	: exergy efficiency (%)

SUBSCRIPTS

Abs	: absorber
AC	: compressor
Coll	: collector
Cond	: condenser

Ev : expansion valve

Evap : Evaporator

Gen : generator

SHES : sensible heat exchanger

SR : solar reservoir

ABBREVIATION*s*

ARC : Absorption Refrigeration Cycle

CCHP : Combined Cooling, Heating, Power

GT : Gas Turbine

H : Heater

HE : Heat Exchanger

HTF : Heat Transfer Fluid

P : Pump

RES : Renewable Energy Sources

SCCHP : Solar Combined Cooling, Heating, Power

SE : Solar Energy

CHAPTER 1

INTRODUCTION

1.1. BACKGROUND AND MOTIVATION

In recent decades, the global energy landscape has undergone a significant transformation driven by increasing energy demand, depleting fossil fuel resources, and mounting environmental concerns [1,2]. The adverse impacts of climate change, such as rising global temperatures and extreme weather patterns, have prompted governments, researchers, and industries to pursue cleaner, more sustainable energy solutions [3,4]. Among the most promising responses is the integration of renewable energy sources into advanced energy systems that can meet multiple demands, electricity, heating, and cooling, through a unified configuration. One such solution is the combined cooling, heating, and power (CCHP) system, particularly when integrated with solar energy as the primary driver [5,6].

One of the most important reactions to this global crisis is the shift to renewable energy sources, which are intrinsically more ecologically friendly and sustainable. Among them, solar energy has emerged as a particularly appealing choice owing to its abundance and scalability [7]. Solar radiation is a massive, limitless energy supply that, when used effectively, may fulfill a considerable amount of the world's energy requirements. Solar energy offers a revolutionary potential to support national energy goals and decrease reliance on imported fuels in areas with high solar irradiation, such as North Africa and the Middle East [8,9]. Solar-driven CCHP systems hold enormous potential to reshape energy delivery mechanisms, especially in regions with abundant solar resources. These systems can achieve energy efficiencies of up to 80% by utilizing waste heat and renewable inputs effectively, making them superior to conventional fossil-fuel-based systems [10].

Libya is blessed with plentiful sunshine; its skies are bright for most of the year, and several places get more than 7 kilowatt-hours of solar energy per square meter each day [11]. Despite this natural endowment, the nation continues to depend nearly completely on oil and gas to satisfy its energy demands. This high reliance has resulted in power shortages, increased energy bills, and environmental damage, particularly in recent years [12,13]. People often encounter power disruptions during hot summers, when cooling demand is greatest, adding to their daily stress. With so much solar energy accessible, there's a huge chance to transition to cleaner, more dependable systems. This research investigates how a solar-powered system capable of cooling, heating, and generating energy simultaneously may be a viable and sustainable option for Libyan villages [14].

Thus, incorporating solar energy into an efficient CCHP system is a compelling answer to Libya's energy difficulties. It not only offers increased energy efficiency and dependability, but it also helps to provide energy security and economic resilience. This research is inspired by the urgent need to investigate and implement renewable energy-based solutions in Libya, and it seeks to give a full analysis of a solar-powered CCHP system adapted to the country's unique climatic, economic, and infrastructural characteristics [6,15].

1.2. PROBLEM STATEMENT

Libya faces many pressing energy challenges threatening its path toward development and long-term economic growth. The country's energy infrastructure remains entirely dependent on fossil fuels, with natural gas and oil being the primary fuels used for power generation, water desalination, and thermal purposes. This reliance on traditional energy sources is becoming unsustainable due to several associated concerns, including fuel price volatility, environmental degradation, inefficient energy conversion, and aging infrastructure.

The energy demand in Libya is steadily increasing, driven by population growth, industrialization, and a rise in the standard of living, all of which are placing an ever-greater burden on the national electricity grid. Particularly in hot summer months, the

energy demand spikes drastically due to the high need for cooling, which constitutes a major share of total residential energy consumption. In many regions, particularly in rural and remote desert communities, the power supply is unreliable or nonexistent, further exacerbating energy poverty and limiting socio-economic progress.

This thesis examines the integration and performance of the solar-based concentrated thermal power (CCHP) approach in the Libyan context, highlighting the technical, social, and economic implications. This is due to several important factors requiring a practical, scalable solution that delivers energy efficiency and environmental conservation. These can be summarized as follows:

- Libya's traditional power generation mostly uses natural gas and oil. This dependency exposes the nation to severe volatility in fuel markets, impeding progress toward energy independence.
- The separate production of power, heating, and cooling wastes significant amounts of input energy. Separate systems often have lower energy efficiency, resulting in greater operating costs and environmental effects.
- Libya's abundant solar energy is mostly unused. While several experimental solar projects have been planned or implemented, large-scale deployment of solar energy solutions is still in its early stages.
- In Libya's hot environment, urban areas, especially those undergoing fast expansion, increasingly rely on air conditioning for comfort. Meeting this need alongside traditional electricity-driven cooling typically puts additional strain on already overburdened networks, generating a loop of greater operating costs and increased emissions.

Despite the country's vast solar energy potential, the use of renewable energy remains low. There is also a significant knowledge and application gap regarding the design and deployment of integrated energy systems, such as solar-powered combined heat and power (CCHP) plants. This research addresses this gap by proposing and evaluating an innovative solar-powered combined heat and power (CCHP) system suitable for Libya. By analyzing the thermodynamic performance of such a system,

this study seeks to provide a practical path towards energy diversification and sustainability in Libya.

1.3. OBJECTIVES OF THE STUDY

The primary goal of this study is to develop, simulate, and assess the performance of a solar-powered Combined Cooling, Heating, and Power (CCHP) system customized for the Libyan setting. To accomplish this goal, the following goals are pursued:

- Design a solar-integrated CCHP system appropriate for Libya's climate and energy demand profile.
- Evaluate the energy efficiency and exergy performance of the proposed system under Libyan climate conditions.
- Investigate the design requirements for solar thermal collectors, heat exchangers, absorption chillers, and power-generation components.

1.4. SCOPE OF THE STUDY

This research is scoped to focus on the design, simulation, and performance analysis of a solar-driven CCHP system. The system configuration includes solar thermal collectors, power generation units, heat exchangers, and absorption chillers. The geographical focus is Libya, and the simulations are based on climatic data reflective of typical Libyan conditions (specifically Tripoli). The study considers:

- A hybrid system consisting of a regenerative Brayton cycle, an absorption chiller, and a heat recovery unit.
- Solar thermal energy is the primary energy source using parabolic trough collectors.
- Thermodynamic modeling based on the first and second laws to evaluate system efficiency.

The study does not include real-life pilot implementation, but the modeling is based on realistic climatic data from Tripoli.

1.5. SIGNIFICANCE OF THE STUDY

This study offers several contributions to academic research and practical energy planning in Libya and other countries with similar solar resources:

- It provides a blueprint for integrating solar energy into advanced multi-functional energy systems.
- It informs Libyan policymakers about viable alternatives to fossil fuel energy systems.
- It demonstrates how thermodynamic analysis can guide the optimal design of sustainable energy systems.
- It contributes to the global body of knowledge on decentralized, renewable-driven CCHP systems.
- It supports international efforts to combat climate change through clean energy transitions.

The significance extends beyond engineering, touching upon economic policy, environmental stewardship, and sustainable development goals.

1.6. OVERVIEW OF COMBINED COOLING, HEATING, AND POWER (CCHP) SYSTEMS

Combined Cooling, Heating, and Power (CCHP) systems, also known as trigeneration systems, represent a significant advancement in energy generation and utilization. Unlike conventional power generation systems that primarily produce electricity and waste the accompanying heat, CCHP systems are designed to capture and repurpose this waste heat for heating and cooling purposes [16,17].

A typical CCHP system consists of the following major components [16,18–20]:

- Prime Mover: This is the core unit responsible for generating mechanical power, which is then converted into electricity. Common prime movers include internal combustion engines, gas turbines, microturbines, and fuel cells.
- Electric Generator: Coupled with the prime mover, the generator converts mechanical energy into electrical energy for on-site use or export to the grid.
- Heat Recovery Unit: The heat recovery system captures the waste heat produced during power generation. This thermal energy can be used for space heating, water heating, or process heating.
- Cooling Unit (Absorption or Adsorption Chiller): The recovered heat can also be utilized to drive thermally activated cooling processes, providing air conditioning or refrigeration. Absorption chillers use a heat-driven cycle (commonly with lithium bromide-water) to deliver cooling, making them ideal for use in CCHP systems.
- Thermal Storage (Optional): Thermal energy storage units (TES) are sometimes integrated into the system to store excess thermal energy, enhancing the system's flexibility and reliability during variable demand periods.

1.6.1. Operation Principle

A solar receiver, often coupled with parabolic troughs or a solar tower, captures concentrated solar radiation and transfers the heat to a working fluid (typically air or helium). The hot working fluid enters a gas turbine, expanding and producing mechanical work that is converted into electricity. After expansion, the exhaust gas, still at a high temperature, passes through a regenerative heat exchanger (recuperator) to preheat the incoming compressed air, improving thermal efficiency. After the recuperator, the remaining thermal energy is recovered in a heat recovery unit to provide useful heat for applications such as water heating, space heating, or industrial processes. A portion of the recovered heat is fed into an absorption chiller or adsorption cooling unit, producing cooling energy (chilled water or air) for buildings or industrial cooling loads [21,22].

1.6.2. Advantages of CCHP Systems

There are many advantages of CCHP systems, and they can be summarized as follows [23–25]:

- CCHP systems use waste heat from power production to produce heating and cooling, with total efficiencies of 70-90%, compared to 30-40% for traditional systems.
- CCHP systems minimize CO_2 and other pollutant emissions by optimizing fuel consumption and reducing waste, aiding climate change mitigation efforts.
- These systems, which generate electricity and use by-product heat, reduce energy expenses for buildings, companies, or communities, particularly in areas with high energy needs.
- Localized generation minimizes reliance on centralized systems and fossil fuel imports, resulting in increased resilience to power outages and fuel price variations.
- CCHP systems often feature backup power capabilities, making them perfect for essential institutions that need continuous energy, such as hospitals and data centers.
- By producing electricity on-site, CCHP systems decrease transmission losses and reduce demand on national power networks.
- They may be customized for a variety of purposes, from hospitals and campuses to residential complexes, making them suitable for both local and large-scale usage.

1.7. SOLAR ENERGY UTILIZATION IN CCHP SYSTEMS

Solar-driven CCHP systems hinge on the availability of high-quality solar irradiation. Solar resource assessment involves analyzing direct normal irradiation (DNI) for concentrating solar collectors or global horizontal irradiation (GHI) for flat-plate collectors and photovoltaics [26–28]. In Libya, the annual solar irradiance ranges among the highest globally, offering abundant potential for large-scale solar integration[29]. The solar thermal collection technologies used for CCHP systems include [30–32]:

- Flat-Plate Collectors: Typically used for low-temperature applications such as domestic hot water or low-intensity process heat.
- Evacuated Tube Collectors: Suitable for moderate temperature ranges and higher thermal efficiency.
- Photovoltaic (PV) Panels: PV panels directly convert sunlight into electricity. In CCHP systems, this electricity can power various components or be fed into the grid. PV systems are becoming increasingly cost-effective, driving interest in self-sufficient energy supplies for buildings.
- Concentrating Collectors (e.g., Parabolic Troughs, Linear Fresnel, Solar Tower): Often employed when higher temperatures are required, such as driving a Brayton or Rankine cycle.

Solar-driven CCHP systems offer a sustainable and efficient solution by combining renewable energy with integrated electricity, heating, and cooling generation, delivering numerous environmental and economic benefits, which summarized as [10,33,34]:

- High overall energy efficiency (electricity + heating + cooling).
- Significant reduction in fossil fuel consumption.
- Reduced energy costs over time.
- Lower greenhouse gas and pollutant emissions.
- Utilization of abundant and renewable solar energy.
- Improved reliability during peak demand and outages.
- Increased energy security and grid independence.
- Supports sustainability and decarbonization goals.
- Low environmental impact compared to conventional systems.
- Scalable for residential, commercial, and industrial use.

1.8. SOLAR-DRIVEN REGENERATIVE BRAYTON CYCLES

The Brayton cycle, commonly used in gas turbine power plants, involves compressing a working fluid (often air), heating it in a combustion chamber (or solar receiver for

solar-driven systems), and then expanding it in a turbine to generate power [35]. Regenerative Brayton cycles feature an internal heat exchanger (the regenerator) that recovers thermal energy from the turbine exhaust to preheat the compressed fluid before it enters the solar receiver or combustion chamber. This significantly improves cycle efficiency by reducing the required heat input [36].

Concentrating solar thermal technology can supply the high temperatures necessary to drive a Brayton turbine. The regenerative component enhances overall efficiency, making more effective use of solar-derived heat. The cycle can be modified to operate in hybrid modes, ensuring consistency of power output during low solar irradiance periods by co-firing natural gas or other fuels [37,38].

When adapting the Brayton cycle to a CCHP configuration, the exhaust heat from the Brayton turbine can be harnessed for process heating, hot water, or driving an absorption chiller [39]. This synergy not only maximizes energy usage but also aligns with the sustainability goals of reduced fossil fuel consumption and minimized carbon emissions.

Libya's solar conditions and high cooling demand make it an ideal candidate for solar regenerative Brayton-based CCHP. Advantages include [40]:

- Daytime operation matches solar peak hours
- Fewer moving parts (especially in closed cycles)
- Efficient use of land in desert zones for solar field installations
- Scalable for institutional, military, or off-grid applications

1.9. ABSORPTION REFRIGERATION SYSTEMS: SUSTAINABLE COOLING SOLUTIONS FOR SOLAR-DRIVEN CCHP APPLICATIONS

Cooling accounts for a significant portion of energy consumption in hot climates. absorption chillers offer a sustainable alternative to conventional vapor-compression systems by using thermal energy rather than electricity [41].

In solar CCHP systems, the recovered heat from the Brayton cycle or solar collectors drives the absorption chiller, enabling efficient cooling without the need for additional power. This integrated approach significantly improves the overall energy utilization of the system [42].

The basic working principle of an absorption refrigeration system relies on the physical and chemical affinity between a refrigerant and an absorbent. The most common working pairs used in commercial systems are water-lithium bromide (H_2O–LiBr) for air-conditioning and ammonia-water (NH_3–H_2O) for low-temperature refrigeration. In the H_2O–LiBr system, water serves as the refrigerant and lithium bromide as the absorbent. The system comprises four main components: the generator, condenser, evaporator, and absorber [43,44].

In the generator, thermal energy (typically from solar collectors or Brayton turbine exhaust) heats the absorbent-refrigerant mixture, causing the refrigerant (water vapor) to separate. The refrigerant vapor then flows to the condenser, where it is cooled and condensed into a liquid. This liquid refrigerant is then expanded and passed into the evaporator, where it absorbs heat from the environment (i.e., provides the cooling effect) and evaporates. The vaporized refrigerant is then absorbed back into the absorbent solution in the absorber, completing the cycle. A solution pump moves the absorbent-refrigerant mixture from the absorber back to the generator, maintaining continuous operation [43].

The integration of absorption systems with solar thermal collectors enables the use of renewable energy for cooling, significantly reducing electricity consumption and greenhouse gas emissions. Various types of solar collectors can be used depending on the required generator temperature. Flat-plate and evacuated tube collectors are suitable for low-temperature applications (80–120°C), while parabolic trough and linear Fresnel collectors are better suited for medium- to high-temperature requirements (up to 200°C or more), which enhance system performance and COP (Coefficient of Performance) [45].

The COP of absorption refrigeration systems generally ranges between 0.6 and 0.8, depending on system design, operating conditions, and the quality of thermal input [46]. Although this is lower than the COP of traditional vapor-compression systems, the ability to utilize waste or solar heat, essentially free or low-cost energy sources, offsets this disadvantage. In solar CCHP systems, where the thermal output from the Brayton cycle or direct solar heating is available, absorption chillers become a cost-effective and environmentally friendly solution for meeting cooling demands.

In Libya, where high ambient temperatures and extended sunshine durations dominate the climate, cooling loads are a major contributor to electricity consumption, especially during the summer months. Conventional air-conditioning systems place a significant burden on the national grid, which already suffers from instability and peak-load issues. By integrating absorption refrigeration systems into solar CCHP designs, it is possible to reduce this burden, enhance overall system efficiency, and shift part of the cooling load from electricity to solar thermal energy.

1.10. OVERVIEW OF LIBYA'S ENERGY CONTEXT

Libya's energy landscape is dominated by fossil fuels, with oil and natural gas accounting for nearly 100% of the electricity generation mix. Despite being rich in hydrocarbons, the country faces periodic electricity shortages and blackouts, especially during peak summer [47–49].

Libya's energy demand has increased steadily over the past two decades, driven by population growth, urbanization, and rising living standards. According to the General Electricity Company of Libya (GECOL), peak electricity demand has reached levels exceeding 7,000 MW in the summer months, far surpassing reliable generation capacity. The residential sector accounts for nearly 40% of total electricity consumption, followed by the industrial and commercial sectors [50,51].

The mismatch between supply and demand often results in rolling blackouts and fuel shortages. In the absence of energy efficiency programs or demand-side management

policies, electricity is heavily subsidized by the government, leading to overconsumption and financial strain on the national economy.

Libya is among the countries with the highest solar irradiation levels in the world. The country receives an average of 3,000 to 3,500 hours of sunshine per year, with daily solar radiation ranging from 6 to 7.5 kWh/m². This exceptional solar resource remains largely untapped. The vast Saharan region provides ample land for the installation of large-scale solar projects, particularly solar thermal power plants and photovoltaic farms [11].

In addition to solar, Libya also possesses potential for wind energy, especially in coastal and inland desert areas. However, the renewable energy contribution to the national energy mix remains below 1%. There are no operational large-scale solar power plants in the country, and only a few pilot projects in distributed solar PV and solar water heating have been implemented, mostly in urban centers.

1.11. STRUCTURE OF THE THESIS

To guide the reader through the breadth and depth of the research, the thesis is structured as follows:

Chapter 1: Introduction

This chapter presents the foundation of the study by outlining the research background, motivation, and objectives, along with the problem statement, scope, and significance. It provides an essential overview of the core concepts relevant to this thesis, including Combined Cooling, Heating, and Power (CCHP) systems, solar energy utilization, and the specific energy challenges and opportunities in the Libyan context. The chapter concludes with a structured outline of the thesis.

Chapter 2: Literature Review

This chapter presents a detailed examination of existing scholarly work on solar-driven CCHP technologies, covering Brayton cycle advancements, absorption refrigeration systems, and relevant case studies worldwide.

Chapter 3: Methodology and Modeling

This chapter outlines the methodological framework adopted for the study, detailing the system modeling approaches, software tools employed, and the procedures for data collection and analysis. It also provides a clear explanation of the key assumptions, defined boundary conditions, and the fundamental equations utilized in the design and simulation of the proposed system.

Chapter 4: Results and Discussions

This chapter presents the results of the performance analysis, discussing system efficiency, cooling capacity, and thermal outputs.

Chapter 5: Conclusions and Future Work

This chapter summarizes the principal contributions of the study, reflecting on how objectives were met. The chapter also suggests directions for subsequent research.

CHAPTER 2

LITERATURE REVIEW

In recent years, the integration of solar energy and hybrid renewable systems into CCHP configurations has gained significant attention. Researchers have focused on developing more efficient, cost-effective, and environmentally sustainable solutions to meet growing energy demands. This chapter reviews and synthesizes key literature on innovative solar-assisted CCHP systems and hybrid energy technologies, providing a foundation for understanding current trends, system designs, and performance optimization methods.

Ehtiwesh et al. [52] investigated the potential of deploying concentrated solar power (CSP) plants in Libya as an alternative and sustainable energy solution. Given Libya's high direct normal irradiation (DNI) and abundant flat land, the research focuses on a 50 MW parabolic trough CSP plant, integrating advanced modeling and analysis methods to assess its feasibility. The study is comprehensive, incorporating exergetic, energetic, economic, and environmental (4E) evaluations of the plant's performance, emphasizing thermodynamic modeling and life cycle assessment (LCA). The methodology involved the development of a computational model using Engineering Equation Solver (EES) to simulate the thermodynamic behavior of both the power cycle (a reheated Rankine cycle) and the solar field. The study also employed Greenius software to conduct an annual performance and economic analysis, comparing different Libyan sites and evaluating the levelized cost of electricity (LCE) under various scenarios. One of the novel contributions of this research is the use of exergetic life cycle assessment (ELCA), combining second-law thermodynamics with traditional LCA to highlight process inefficiencies and environmental hotspots. The analysis revealed that the solar field is the most critical component, contributing 79% to the overall impact, with steel, molten salt, and synthetic oil being the materials with

the highest exergetic demand. CSP shows significantly lower environmental impact than fossil-fuel-based systems like natural gas and oil plants. The study further explored thermal energy storage (TES), specifically thermocline systems, to enhance dispatchability and reduce operational costs. A numerical model for the thermocline storage tank is developed and validated, showing promising alignment with experimental data and potential for cost-effective electricity generation even during non-solar hours. The findings supported the viability of CSP deployment in Libya, highlighting its technical and economic advantages and reinforcing the country's potential as a strategic exporter of renewable electricity to Europe. The integrated 4E approach offers a robust framework for future CSP planning and policy in sun-rich regions.

Tawil et al. [53] explored the current state, challenges, and opportunities of using solar energy for space heating, cooling, and ventilation in Libyan residential buildings. It consolidates findings from a wide range of academic studies, technical reports, and field investigations to assess how active and passive solar systems can be applied to improve thermal comfort and reduce electricity consumption in Libya's climate. The paper highlighted the growing energy demands in Libya's residential sector. The study categorized solar energy applications into active systems (e.g., solar collectors, absorption chillers, Rankine refrigeration systems) and passive systems (e.g., thermal mass, natural ventilation, Trombe walls, earth-sheltered designs). It discussed several case studies from Libyan cities like Ghadames, Gharyan, Sabha, and Tripoli, showing how traditional building designs using local materials and smart orientations naturally regulate indoor temperatures more efficiently than modern structures. Furthermore, the research presented experimental simulations, modeling approaches, and field surveys that evaluate the performance of solar-assisted HVAC technologies. It emphasized the potential of combining solar thermal collectors, storage systems, and energy efficiency measures to create integrated solutions for Libyan housing. Key findings suggest that traditional architectural practices, if adapted and combined with modern solar technologies, can significantly improve energy efficiency, reduce CO_2 emissions, and support sustainable development.

Ehtiwesh et al. [54] presented a dynamic model of a direct steam generation (DSG) solar power system integrated with a steam accumulator to meet the electricity and hot water needs of a hospital in Murzuq, Libya, under real climate conditions. The system used PTC to generate superheated steam that powers a Rankine cycle directly. The control system regulated the pump flow and steam pressure using throttle valves to match the hospital's hourly energy demand, which peaks at 200 kW during the day and drops to 50 kW at night. Key components modeled include the solar collector field, steam turbine, steam accumulator, DHW heat exchanger, condenser, and control systems. The simulation results showed that the system achieves a maximum thermal efficiency of 23% during peak solar hours and 20% during night using stored steam.

Wang et al. [55] presented a multi-objective optimization of a solar-driven CCHP system that integrates an ORC with an ejector refrigeration cycle. The system used flat-plate solar collectors and a TES tank to meet users' electricity, cooling, and heating demands throughout the year. The optimization balanced performance (useful output) with economic factors (total heat transfer area) across three operational modes: power-only, CHP, and CCP. A comprehensive mathematical model was developed to simulate system behavior, incorporating thermodynamic principles and performance criteria. The decision variables included turbine inlet temperature and pressure, condenser temperature, and pinch temperature difference in the vapor generator. The study applied the Non-dominated Sorting Genetic Algorithm II (NSGA-II) for optimization. Key results showed optimal daily average efficiencies of 13.81% in CHP mode, 9.75% in power mode, and 8.76% in CCP mode. Exergy efficiency peaked at 8.41% in CHP mode. Optimal outputs and heat transfer areas were CHP Mode: 8.89 kW and 38.78 m^2; Power Mode: 6.40 kW and 46.16 m^2; and CCP Mode: 5.84 kW and 58.74 m^2. The results demonstrated that no single configuration optimally satisfies all objectives, and trade-offs are essential. The Pareto front approach enables the selection of a balanced solution based on user priorities. The study concludes that multi-objective optimization is crucial for designing efficient and economically viable solar-driven trigeneration systems.

Saini et al. [56] Saini et al. [5] proposed and evaluated three novel configurations of solar-driven CCHP systems, using evacuated tube collectors (ETCs) for solar thermal

input, an Organic Rankine Cycle (ORC) for power generation, and an Ejector Refrigeration Cycle (ERC) for cooling. All configurations also include a heat exchanger for delivering useful heat. The objective is to identify compact, efficient, and eco-friendly CCHP solutions using n-butane as the working fluid under varying operational conditions. Each configuration differs in the way components like generators, condensers, and ejectors are integrated. The results reveal that configuration 1 achieves the highest power output and exergy efficiency, configuration 2 provides the maximum cooling capacity, and configuration 3 delivers the best overall performance, with the highest performance index, compactness, and flexible operation in all seasons. The study also finds that the ETC is the largest source of irreversibility (over 91%), and configuration 3 is the most balanced solution for year-round operation, offering combined power, cooling, and heating capabilities with fewer components.

Chen et al. [57] presented a detailed analysis and simulation of a solar-driven combined CCHP system that integrates an ORC and a double-effect absorption heat pump (AHP) to provide electricity, cooling, space heating, and domestic hot water. The system also utilized geothermal energy (GE) for enhanced thermal efficiency. PTCs served as the primary solar energy input, cascading thermal energy between the ORC and AHP. Using dynamic simulations and models, the researchers evaluated energy, exergy, and exergo-economic performance across three seasonal operating modes: heating, cooling, and transition. The system achieved a COP of 1.38–2.37, annual energy efficiency of 56.5%, and exergy efficiency of 9.6%. The payback period is notably short at 3.5 years, and the specific cost of electricity is calculated at 0.12 $/kWh, lower than traditional systems. The AHP product costs were higher, especially for domestic hot water (0.31 $/kWh), due to low exergy levels and high component costs. A sensitivity analysis revealed that the system’s performance is most influenced by solar irradiance, absorber inlet/outlet temperatures, and distribution of operational modes (cooling vs. heating periods). Results indicated that the cooling mode provided the highest exergy efficiency, while heating yielded the highest energy efficiency. The ORC unit was responsible for most electricity production, while the AHP dominated thermal outputs. The PTC showed the highest exergy losses, indicating a target for future system improvement.

Wang et al. [58]introduced and analyzed a novel solar-driven CCHP system that integrates a Rankine cycle (RC) with an ejector refrigeration cycle (ERC). The system is powered by compound CPCs chosen for their high thermal efficiency and large acceptance angle. The system is designed to generate electricity, cooling, and useful heat simultaneously, offering a promising alternative to traditional CCHP systems that rely on fossil-fuel-based prime movers like gas turbines (GTs) or internal combustion engines (ICEs). The model incorporated a sensible heat storage tank, a TES system, and auxiliary heating to maintain continuous operation under variable solar conditions. The ERC, known for its simplicity and low maintenance, provided cooling using waste heat from the RC. The study emphasized the impact of PTC orientation (slope and hour angle) on system performance and demonstrated that a slope angle of 60° at midday yielded the highest exergy efficiency. Through thermodynamic modeling and genetic algorithm (GA)-based optimization, the study achieved a maximum exergy efficiency of 60.33% under optimal conditions. The performance analysis showed that the net power output reaches 17.38 kW, the heating output 77.51 kW, and the cooling output 4.44 kW, all driven by solar input.

Cisek et al. [59] introduced the RESHeat software to facilitate the preliminary design and assessment of solar-driven CCHP systems. Unlike traditional dynamic simulation tools that require advanced expertise and computational power, RESHeat simplifies the design process using one-dimensional mathematical models, making it accessible for engineers, policymakers, and commercial partners. The software integrates renewable energy (RE) components such as thermal energy storage, PTC solar collectors, photovoltaic (PV) panels (TES), and heat pumps, enabling users to assess energy efficiency, economic feasibility, and environmental impact. The study validated the tool by comparing it with Polysun simulations, achieving accuracy with less than 20% deviation. Key features of RESHeat included a modular structure that supports quick configuration of building types, climates, and system components. Cooling and heating load calculations based on dynamic outdoor temperature duration curves and energy demand simulations for residential and public buildings using predefined parameters. The system was tested across various European climates and demonstrated strong potential to reduce CO_2 emissions by over 60% compared to traditional systems.

Zhang et al. [60] proposed an innovative design and optimization approach for a combined CCHP system that combines photovoltaic (PV) and biomass (biogas) energy. The focus was on rural and island regions with limited energy access, where renewable hybrid systems offered a practical and sustainable solution. The system configuration included a biogas ICE acting as the power generation unit (PGU), a PV array for direct solar electricity production, electric and absorption chillers for space cooling, a biogas boiler for additional heat generation, and heat exchangers and storage for thermal management. The three primary performance indicators are Primary Energy Saving Ratio (PESR), Annual Total Cost Saving Rate (ATCSR), and Carbon Emission Reduction Ratio (CERR). A case study was conducted on a farm in Jinan, China, demonstrating the model's feasibility. Optimal results for the system under standard conditions were PESR = 20.94% (indicating significant energy savings), ATCSR = 11.73% (economic viability), and CERR = 40.79% (substantial reduction in emissions). The simulation accounts for seasonal variation, biogas availability, PV output fluctuations, and load demands across heating, cooling, and electrical consumption. The system dynamically balances on-grid and off-grid modes, allowing excess solar energy to be stored or sold to the grid and compensating with biogas energy when needed. Key findings highlighted that integrating solar and biomass resources improves energy security, reduces reliance on fossil fuels, and provides a sustainable, decentralized energy solution for small-scale communities. The results suggested policy implications for broader adoption, particularly in developing or remote areas lacking centralized energy infrastructure.

Liu [61] proposed a novel hybrid CCHP system that integrates solar-driven biomass gasification with a solid oxide fuel cell (SOFC) and a homogeneous charge compression ignition (HCCI) engine to produce electricity, heating, and cooling in a highly efficient and sustainable manner. The system uses dish-type solar collectors to supply thermal energy for gasifying biomass, producing a hydrogen-rich syngas. This syngas powers an SOFC, which generates electricity at high efficiency. Unused fuel and exhaust gases from the solid oxide fuel cell (SOFC) are directed to the HCCI engine for further energy recovery. The remaining heat is captured and used in a double-effect ARC for space cooling and to provide domestic hot water. Key findings

of the study showed that the energy efficiency was up to 57.5%, significantly higher than conventional systems. Exergy efficiency reached 36.6%, thanks to the efficient use of high-temperature energy. The system reduced CO_2 emissions by 46.3%, enhancing its environmental performance. Biomass utilization was increased by over 60%, showing improved renewable fuel use. Exergoeconomic analysis indicated that SOFC is the most cost-effective component, while cooling was the most exergy-intensive. The study concluded that the system is technically viable and environmentally sustainable, especially for regions rich in solar energy and biomass resources.

Salimi et al. [62] provided a comprehensive evaluation of the environmental performance of CCHP systems, emphasizing their potential to reduce greenhouse gas emissions, energy consumption, and water use compared to conventional energy systems. The review explains that CCHP systems enhance overall efficiency by recovering waste heat from power generation to provide heating and cooling, significantly lowering environmental impacts simultaneously. However, the extent of these benefits depends heavily on the type of energy input (fossil vs. renewable), system configuration, and operational control strategies. Life cycle assessment (LCA) studies cited in the paper reveal that renewable-integrated CCHP systems, especially those powered by solar, biomass, or geothermal energy, can considerably reduce the carbon footprint. Solar-assisted systems perform well in sunny climates, while biomass offers a consistent supply regardless of weather variability. The review also addressed the water footprint, showing that CCHP systems consume much less water than traditional systems, especially when thermal load-following strategies are used. Policy instruments like carbon taxation are also discussed as effective tools to encourage clean CCHP operation, with an optimal carbon tax estimated at $10/kWh. The authors recommend further improvements in technology components, integration of energy storage, and intelligent control systems to maximize the environmental and economic performance of future CCHP installations.

Haghgh et al. [63] presented a thermodynamic analysis of a novel solar-driven CCHP system designed for the summer air-conditioning needs of the School of Engineering at Urmia University, Iran. The system utilized PTSCs as the primary heat source,

which drove an ORC to produce electricity, heating (hot water and steam), and cooling (via two single-effect absorption chillers using LiBr–H_2O). The performance of the system is evaluated under three operational modes: Solar Mode (PTSCs directly supply heat), Solar + Storage Mode (PTSCs and storage tanks work together), and Storage Mode (heat is provided entirely from the thermal storage). Under varying solar radiation, the system achieved energy efficiencies of 98% (solar and storage), 47.3% (solar + storage), and 98% (storage), and exergy efficiencies of 17%, 8.3%, and 17%, respectively. The maximum energy loads observed for summer air conditioning were 896.9 kW cooling, 228.5 kW heating, and 1500 kW electricity, supported by up to 1625 PTSCs throughout the year. A detailed parametric analysis revealed the influence of ORC pump temperature and turbine inlet pressure on system performance. As inlet temperatures rose, thermal efficiency increased, but exergy efficiency decreased due to greater irreversibility. The study also validated its model using data from previous works and Sandia National Laboratories, confirming its accuracy.

Sainiet al. [64] presented and evaluated a compact, solar-powered CCHP system tailored for small buildings in remote areas. The system combines evacuated thermal energy storage (TES), tube collectors (ETCs), an ejector refrigeration cycle (ERC), an organic Rankine cycle (ORC), and a water heater. The innovation lay in its low component count, suitability for year-round operation, and adaptability to solar intermittency via latent heat TES using HDPE as phase change material. Using n-butane as the working fluid, the system delivers electricity (via ORC), cooling (via ERC), and heating (via the water heater). The vapor generator divides vapor into turbine and ejector streams, optimizing energy extraction. A rigorous thermodynamic model was developed in Engineering Equation Solver (EES), complemented by economic and environmental analyses. The results proved that the exergy efficiency was 3.16% overall, the ETC exergy efficiency was 10.18%, and the heating cycle was 39.80%. Annual costs: $2023 total, with 119.9 $ (power), $134.3 (cooling), and 1769 $ (heating). Carbon savings: Equivalent CO_2 emissions of 13.10 tons/year (vs. coal power). Irreversibility: The highest in solar collectors (89.82%), followed by water heaters, ejectors, and vapor generators. Parametric analyses reveal that increasing generator and evaporator temperatures boosted exergy efficiency and heating output while reducing cooling and power costs. Conversely, higher condenser temperatures

degrade efficiency and raise emissions. Turbine mass fraction tuning influenced output ratios, with 50% achieving a balance between cooling and power costs. Overall, this system offered an environmentally friendly, cost-effective, and scalable solution for decentralized energy generation.

Wang et al. [65] presented a novel CCHP system that integrates SOFC, an ORC, solar energy storage, methanol thermochemical hydrogen production, and a double-effect AR/HP. The core innovation lay in decoupling cooling/heating from power outputs, enabling greater flexibility and efficiency to meet fluctuating user loads. The system used PTCs to heat a thermal oil circuit that stores and supplies energy. Methanol is decomposed into hydrogen-rich syngas, which powers a SOFC to produce electricity. Waste heat from the SOFC and gas turbines is recovered by the ORC and AR/HP to provide additional electricity, heating, cooling, and domestic hot water (DHW). Two operational strategies are analyzed: grid-assisted cooling, which supplements with purchased electricity, and the extra methanol strategy, which uses additional fuel to meet peak cooling demands. The key findings showed that energy efficiency reached 96.96%, while exergy efficiency peaked at 19.31%. Fuel savings improved by 19.1% compared to prior systems. Carbon emissions vary seasonally: 144.07 g/kWh in summer (grid strategy), 81.74 g/kWh (methanol strategy), and as low as 15.76 g/kWh in the transition season.

Zhao et al. [66] presented a comparative analysis of three configurations of solar-driven ORC-based CCHP systems: Sequential System (SS), Parallel System I (PS-I), and Parallel System II (PS-II). Each configuration combines PTCs with a single-effect absorption chiller (AC) and a heat exchanger for energy delivery. The SS configuration uses an energy cascade strategy, where waste heat from the ORC is reused for heating and cooling, resulting in high thermodynamic efficiency and compact size. In contrast, PS-I and PS-II distribute heat in parallel, offering greater control and flexibility but at the cost of higher investment and system size. The study developed a multi-criteria optimization model that integrates thermodynamic, sizing, and economic analyses using MATLAB and REFPROP tools. The Organic Rankine Cycle (ORC) system was standardized at a 200 kW capacity across all scenarios. Five working fluids were evaluated, with hexamethyldisiloxane (MM) identified as the optimal choice for the

SS configuration, and R123 selected for the PS configuration. Key results indicated that for the SS system, the annual outputs reached 369 MWh of power, 1650 MWh of heating, and 1940 MWh of cooling, achieving an overall efficiency of 45.82%. The SS configuration also exhibited the shortest payback time (PBT) at 7.43 years and the lowest associated costs. In contrast, the PS-I system produced a higher power output of 878 MWh but recorded a lower overall efficiency of 38.3% and a longer PBT of 9.23 years. The PS-II configuration showed the weakest performance, with an efficiency of 33.81% and a PBT of 10.18 years.

Xia et al. [67] introduced and optimized a novel solar-driven Direct Heating and Cooling (DHC) system that incorporates a transcritical carbon dioxide heat pump (TCHP), evacuated tube solar collectors (ETC), and photovoltaic (PV) panels. This study focused on improving how buildings meet their thermal energy needs by making the process more efficient, economical, and environmentally friendly. It uses an exergoeconomic optimization method that adapts to real-time building demands and changing environmental conditions. The system is designed to operate in two distinct modes: during heating periods, it uses evacuated tube collectors (ETCs) and photovoltaic (PV) panels to power the TCHP unit; during cooling periods, it relies on PV-generated electricity and ground source water (GSW) as a heat sink. A real-world application was tested on a 3000 m² building in Harbin, China, equipped with 226 ETCs and 390 m² of PV modules to evaluate the system's performance. The findings showed that optimal discharge pressures were 7.31 MPa (heating) and 8.93 MPa (cooling). The lowest total UEC is 0.629 $/kWh (reduced by 43.56% from the benchmark). Annual energy & exergy efficiencies: 40.30% and 1.81%, respectively. The highest energy loss is PV (325 kW in heating), accounting for 72%. Exergoeconomic factors: 100% for PV, ETC (solar input is free), and 38.2% for TCHP. Sensitivity analysis revealed that increasing DNI lowers UEC and improves efficiency, and a higher sold electricity ratio reduces energy/exergy efficiency but increases UEC. The results confirm the feasibility of applying this solar-based DHC system to buildings such as hotels, hospitals, and schools, especially where cooling and heating demands exist. The developed method integrates building loads directly into optimization, ensuring better economic and environmental performance across seasons.

Zarei et al. [68] proposed and evaluated a novel solar-CCHP system that utilizes photovoltaic thermal collectors (PVT) and PTCs in a series configuration to maximize solar energy harvesting. The system included a regenerative ORC for power generation and an ejector–vapor compression refrigeration cycle (VCRC) for dual-temperature cooling. Designed primarily for domestic use, the system supplies refrigeration (above and below zero), space heating, and electricity using eco-friendly working fluids like R123 and R290. Water from the PVT unit pre-cools the VCRC condenser and preheats before entering the PTC, reducing collector size and cost. This high-temperature water then drives the ORC cycle. The system's novel configuration ensures thermal and electrical efficiency, using recovered heat in a regenerative loop to enhance performance. The results showed that the maximum energy and exergy efficiencies were 75.6% and 10.77%, respectively, using R123. Optimal water mass flow rate significantly impacts COP and overall system performance. Variable flow rate control maintained system efficiency under varying solar irradiance (G = 500–1000 W/m²). A daily performance case study conducted in Tehran demonstrated a peak power output of 563.8 W and achieved a hot water temperature of 82.1°C. The system showed strong economic viability, with an estimated payback period of approximately 6.4 years, outperforming comparable systems reported in the literature regarding cost-effectiveness. The study concludes that this multi-source solar CCHP system is a feasible, efficient, and sustainable solution for zero-energy buildings, offering notable improvements in environmental performance and cost-efficiency for residential energy needs.

Li et al. [69] proposed a novel multi-dimensional day-ahead optimization model for a community-scale solar-driven CCHP system, integrated with demand-side management (DSM) and generalized energy storage (GES). Unlike prior studies focusing only on either system-side or user-side optimization, this model combines both, integrating flexible resources such as electric vehicles (EVs), batteries, electro-to-thermal (E2T) devices, and shiftable heating/cooling loads. The GES framework allows dynamic energy demands and resource utilization management, enabling real-time interaction between users and the energy system. The optimization process assesses the system's performance based on four main objectives: minimizing

economic cost, managing load fluctuations, and maximizing energy and exergy efficiencies. The results indicated that the load fluctuation was reduced by 54%, improving operational stability. Energy efficiency improved by 2.5%, exergy efficiency by 8.7%, and economic performance by 2.4%. Scene C3 (load fluctuation-focused) scored highest across most scenarios due to smoother grid interaction and reduced dependence on external power. DSM allowed for load shifting, particularly EV and battery usage during off-peak periods, reducing grid costs and enhancing equipment efficiency. This study emphasized the importance of co-optimizing system and user-side flexibility for future urban energy systems. The findings contribute to the design of low-carbon, resilient, and cost-effective microgrids capable of adapting to variable renewable energy and user behavior.

Bataineh et al. [33] presented a comprehensive review of hybrid fuel-assisted solar-powered Stirling engine (SE)-based CCHP systems, focusing on their design, operation, performance, and optimization. Stirling engines, due to their external combustion design, low emissions, fuel flexibility (solar, gas, biomass), and high reliability, are highlighted as strong candidates for micro- and small-scale CCHP systems in buildings and distributed energy systems. The study outlined system configurations where a solar dish Stirling engine (SE) generates electricity, and the waste heat is recovered for cooling and heating through ACs. When solar radiation is insufficient, hybridization with fossil fuels or biofuels ensures operational continuity. System modeling, including energy, exergy, and economic assessments, reveals overall efficiencies up to 96%, with thermal efficiencies reaching 70–80% and electrical efficiencies up to 30% in optimized setups. Key challenges addressed included power control and integration complexity, low specific power output compared to ICEs, high initial capital cost, and integration of storage and control systems. The review summarized performance indicators such as primary energy saving ratio (PESR), CO_2 emission reduction, and levelized cost of energy (LCOE). It also compares theoretical and empirical Stirling engine models, including Beale and West correlations. It reviews real-world applications, including field-tested systems in Germany, France, the USA, and China.

Huang et al. [70] evaluated the techno-economic performance of seven energy storage configurations integrated into renewable energy-based RCCHP systems. As the global shift away from fossil fuels accelerates, integrating energy storage becomes critical to manage the variability of renewables such as solar PV. The authors compared configurations involving battery (BAT), thermal energy storage (TES), and hydrogen storage (HS), both individually and in combination, to determine the most cost-effective solutions under varying self-sufficiency rates (SSR) and grid-connectivity scenarios. Using Mixed-Integer Linear Programming (MILP) for optimization and full-year time series data from a simulated community in Texas, the study showed BAT+HS+TES is the most cost-effective configuration at 100% SSR, lowering annualized total cost (ATC) by up to 39.5% compared to single-storage options. No storage is needed at SSR < 40%; TES provided the cheapest augmentation until ~60% SSR. HS was critical in absorbing long-term PV variability for full off-grid operation due to its lack of self-loss and long-duration storage capability. BAT is ideal for intraday storage, while TES (hot and chilled water tanks) offers low-cost short-term thermal balancing.

Nami et al. [71] presented a thermodynamic and sustainability analysis of a novel 1 MW solar-assisted biomass-based CCHP system tailored for domestic applications. The system incorporated an externally fired GT, a steam RC, concentrated photovoltaic thermal (CPVT) panels, and a lithium-bromide absorption chiller to meet electricity, space heating, domestic hot water, and cooling demands. The system utilized paper biomass as the fuel source and solar energy via CPVT for both electricity generation and thermal augmentation. The gas and steam turbines are the main power units, while heat exchangers and a chiller recover and utilize waste heat for heating and cooling. A pressurized water circuit collects heat from the steam condenser and CPVT to deliver hot water and space heating. The system was modeled using EES with detailed exergy and sensitivity analyses. The key performance results of the system demonstrated a well-balanced and efficient energy output across multiple functions. The system delivered a net electrical output of 1,000 kW. Additionally, it provided substantial thermal energy for space heating at 1,241 kW. Furthermore, the system supplied 101.5 kW for domestic hot water. Lastly, it featured a cooling capacity of 55.35 kW. Overall thermal, electrical, and exergy efficiencies were 82.1%, 34.23%,

and 35.23%. Highest exergy destruction occurs in the CPVT due to temperature mismatches. The gasifier, combustion chamber, and Rankine cycle components (HRSG, ST, condenser) also show significant exergy losses. System optimization showed that an air compressor pressure ratio of 8.8 and a GT inlet temperature of 1400 K offer optimal performance. Winter operation is more efficient than summer due to higher utilization of heat. In summer, increased cooling demand slightly lowers exergy and thermal efficiency. The study concluded that such a solar-biomass CCHP system is thermodynamically viable for domestic-scale decentralized energy supply, especially in regions with solar availability and biomass access.

Wu et al. [34] introduced a novel hybrid CCHP system that integrates solar thermochemistry with natural gas reforming to produce syngas for use in an ICE-based trigeneration setup. The system is designed to enhance energy efficiency and reduce natural gas consumption by converting solar energy into chemical energy through a solar-driven reforming reactor. This allowed the system to store solar energy in syngas, overcoming the limitations of solar intermittency and improving operational stability. A genetic algorithm (GA) is used to optimize key system parameters (engine capacity and solar field area) with objectives covering energy savings (APES), economic cost savings (ATCS), and CO_2 emissions reduction (CDER). The system's performance was assessed across five climatic zones in China (Harbin, Beijing, Shanghai, Kunming, and Guangzhou) using hourly building load data and solar radiation profiles. Evaluating the system’s performance in Harbin indicated substantial environmental and economic advantages. The primary energy saving (APES) reached an impressive 69.76%. The system achieved a total cost saving (ATCS) of 49.80%. The CO_2 emission reduction (CDER) amounted to 71.55%. Best performance in cold zones due to high solar availability and large heating demands. Harbin had the highest solar share (22.5%) and best comprehensive performance (CP ≈ 64.75%). Syngas production efficiency peaked at ~67.5% at 900°C. Seasonal performance analysis revealed that the system performed better in winter than summer, mainly due to the higher heating demand and more effective utilization of available solar energy during the colder months. The sensitivity analysis revealed that electricity price is the most impactful factor on system performance, followed by natural gas and solar field cost. The study concludes that solar thermochemical hybrid CCHP systems are well-suited for

northern climate zones with high heating loads and can significantly reduce dependency on conventional fuels.

Behzadiet al. [72] investigated a novel solar cogeneration building energy system that utilizes PVT panels and a heat storage tank, integrated with three types of district heating (DH) systems: 3rd generation (3GDH), low-temperature (LTDH), and ultra-low-temperature (ULTDH). Designed for affordability and efficiency, the system omits expensive components like heat pumps and batteries, offering households a cost-effective renewable energy solution. The system was dynamically simulated using TRNSYS software for a single-family house located in Esbjerg, Denmark, incorporating real hourly weather conditions and actual energy demand data. The system supplied electricity, space heating, and domestic hot water (DHW). The energy flow is prioritized in-building usage, and surplus is sold to the grid or DH network. The analysis revealed that the ULTDH system (Model a) significantly outperformed alternative systems in multiple performance aspects. It achieved the highest electricity production at 3647.4 kWh, notably surpassing LTDH (2279.6 kWh) and 3GDH (911.8 kWh). Furthermore, the system generated substantial thermal energy, with heat generation reaching 9118.5 kWh, supporting heating and hot water applications. Additionally, the system delivered 402.86 m^3 of surplus hot water. The highest overall system efficiency was 70%, compared to 59.5% for LTDH and 49% for 3GDH. Lower DH temperatures led to higher PVT efficiency due to reduced panel temperature. In colder months, the system alone can't meet heating needs; external grid support is required. Surplus electricity is sold in summer and spring; grid imports are necessary in winter.

Borhani et al. [73] comprehensively evaluated a solar-powered CCHP (S-CCHP) system designed for residential energy needs. The system integrated PVT collectors, an auxiliary heater, an AC, and hot/cold storage tanks, which are dynamically simulated using TRNSYS software. It also featured an Artificial Neural Network (ANN) model to accurately forecast system performance under different regional climates in Iran, reducing simulation time. Five cities representing different climatic zones (Ahvaz, Tehran, Yazd, Ramsar, and Hamedan) were analyzed. Ahvaz, with its hot climate, achieved the highest total annual efficiency (13.27%) and annual power

generation (28,432.17 kWh), while Yazd achieved the highest solar fraction (91.97%) due to its intense solar radiation. In contrast, Ramsar had the lowest efficiency (11.35%) and solar fraction (41.51%). The artificial neural network (ANN) was trained using 1,825 simulation data samples and validated through performance metrics such as R^2 (reaching up to 0.999), mean squared error (MSE), and root mean square error (RMSE), confirming its excellent prediction accuracy for electrical (EPP), heating (HPP), and cooling power production (CPP). The most effective ANN architecture identified was 4×10×4, which demonstrated strong generalization across different climatic conditions and significantly reduced computation time—from nearly 4 hours down to just 2.3 seconds. The results indicated that warm climates like Ahvaz are optimal for implementing this solar-based trigeneration system. The use of ANN enables real-time performance forecasting.

Herrando et al. [74] explored and compared the technoeconomic performance of various S-CCHP systems, particularly focusing on those using hybrid PVT collectors. A case study conducted at the University Campus of Bari in Italy evaluated the performance of three different systems: an innovative S-CCHP system equipped with flat-box PVT collectors, a conventional system using evacuated tube collectors (ETCs) for heating and cooling (SHC), and a standalone PV system dedicated to electricity generation. The proposed S-CCHP system incorporates PVT collectors, a stratified hot water storage tank, a LiBr-H_2O absorption chiller, and conventional gas boilers for backup heating. This hybrid configuration demonstrated the system's potential to fulfill building energy demands partially. Specifically, it covers 20.9% of the space heating load, 55.1% of the cooling demand, and 16.3% of the electricity requirements. While the PVT-based system had a higher upfront cost than the PV-only system, it delivered greater environmental benefits, saving up to 911 tons of CO_2 annually and 5,460 MWh of primary energy, 16% and 12% more than the PV system. In contrast, the ETC-based system, although cheaper, lacks electricity generation and shows lower environmental and economic benefits. The payback time (PBT) of the PVT-based S-CCHP system was 16.7 years, versus 6.1 years for the PV system and over 37 years for the ETC system, assuming current Italian utility prices. However, if utility prices rise (e.g., to Danish levels), the PBT for the S-CCHP system could drop to 10.2 years, enhancing its financial viability. Key insights from the analysis highlight several

important system design and implementation considerations. One major limitation identified is the impact of restricted roof space, which significantly affects system sizing and overall performance, especially in urban settings. Furthermore, PVT systems are more effective when applied to buildings with concurrent thermal and electrical energy demands. Additionally, introducing novel flat-box polycarbonate PVT collectors enhances thermal efficiency while contributing to cost reduction. The study concludes that while the S-CCHP system has a longer payback time than PV systems, its dual energy output and higher sustainability performance make it a promising candidate for urban decarbonization strategies.

García-Domínguez et al. [75] investigated the thermodynamic performance of a solar-driven trigeneration system using a regenerative, recuperated, and superheated ORC integrated with a single-effect H_2O/LiBr absorption heat pump. The system is powered by Solar PTCs, and the novelty lies in applying a new exergy methodology that calculates dead states individually for each subsystem, enhancing analysis accuracy. The presented system integrates an ORC for electricity generation and an absorption heat pump to meet heating and cooling demand. The ORC electrical output was 82.1 kW, while the system delivers 200.4 kW of cooling and 471.7 kW of heating. It achieved an exceptionally high overall energy efficiency of 152.4%. However, the overall exergy efficiency stands at 21.1%. The ORC exergy efficiency reached 84.9%. The analysis also identified the solar PTCs as the main source of exergy destruction, accounting for 73% of total losses.

Chen et al. [76] proposed and evaluated a solar-powered trigeneration system that integrates a regenerative, recuperated, and superheated ORC with a single-effect H_2O/LiBr absorption heat pump, both driven by SPTCs. The system demonstrated robust multi-functional performance by simultaneously providing electricity, heating, and cooling. It generated 82.1 kW of electricity, delivered 200.4 kW of cooling output, and supplied 471.7 kW of thermal energy for heating. The overall energy efficiency of the system reached an impressive 152.4%. In terms of thermodynamic quality, the system achieved an overall exergy efficiency of 21.1%, while the electrical-exergy efficiency is measured at 17.5%. Notably, the ORC component alone exhibited an exergy efficiency of 84.9%. The main source of exergy destruction was the PTC solar

collector field, responsible for 73% of the input exergy losses, mainly due to high thermal gradients and optical losses. The absorption heat pump and ORC contributed to 10% and 5% of destruction, respectively.

Aieneh et al. [77] presented a novel standalone solar-powered CCHP system designed for continuous production of electricity, heating, cooling, and hydrogen, integrating an ejector refrigeration cycle (ERC), a supercritical CO_2 Rankine cycle, and a PEM electrolyzer. The system was powered entirely by a solar tower and heliostat field, and a comprehensive 3E analysis was performed to evaluate its efficiency and cost. The system's key performance metrics reflected a balanced and multifaceted energy solution. It achieved an energy efficiency of 40.61% and an exergy efficiency of 33.50%. The net power generation reached 11.7 MW, complemented by a substantial heating load of 13.92 MW and a cooling load of 2.6 MW. Additionally, the system supported hydrogen production at 12.95 grams per second. From an economic perspective, the system operates at a cost rate of 2875.74 USD/hour, with a cost per exergy unit of 25.65 USD/GJ. These indicators confirm the system’s potential for high-performance, cost-effective, sustainable energy deployment. Exergy destruction is the highest in the heliostat mirrors (20 MW) and receiver (10.11 MW), while cost-heavy components include the PEM electrolyzer and heliostat array. The system's strength lies in its zero-emission, continuous operation, made possible by PCM-based thermal storage and integrated hydrogen production. The study concluded that this hybrid system significantly outperforms many existing solar-driven CCHP configurations in efficiency and flexibility.

The following table summarizes key recent studies focused on solar-driven combined cooling, heating, and power (CCHP) systems, as well as hybrid renewable energy technologies. Each entry highlights the study focus, system configuration, and major findings. This comprehensive overview provides valuable insights into the advancements, challenges, and optimization strategies being explored in the field of sustainable energy

Table 2.1. Summary of recent literature on solar-driven CCHP and renewable energy systems

No.	Authors	Focus of Study	System/Technology	Key Outcomes
1	Ehtiwesh et al. [52]	Feasibility of CSP plants in Libya	Parabolic Trough CSP + 4E Analysis	High solar potential, ELCA shows environmental advantages, 79% impact from solar field materials
2	Tawil et al. [53]	Solar heating/cooling in Libyan buildings	Active & Passive Solar Systems	Traditional designs improve efficiency, solar HVAC integration recommended
3	Ehtiwesh et al. [53]	DSG system for hospital energy needs	PTC with Steam Accumulator	Achieved 23% thermal efficiency peak
4	Wang et al. [54]	Solar-driven CCHP optimization	ORC + Ejector cycle + TES	Optimal energy modes with trade-offs, Pareto optimization
5	Saini et al. [55]	Novel CCHP system topologies	ETC + ORC + ERC	Configuration 3 best overall; ETC has 91% irreversibility
6	Chen et al. [56]	Solar-driven CCHP with geothermal	ORC + AHP + PTC	56.5% energy efficiency, 3.5 years payback
7	Wang et al. [57]	Solar CCHP with CPC collectors	RC + ERC + TES	60.33% maximum exergy efficiency
8	Cisek et al. [58]	Simplified design tool for CCHP	RESHeat Software	Modular tool, <20% deviation compared to Polysun
9	Zhang et al. [59]	PV–Biomass hybrid CCHP	Biogas ICE + PV + Absorption Chiller	20.94% PESR, 40.79% carbon emission reduction
10	Liu et al. [60]	Solar biomass hybrid CCHP	SOFC + HCCI engine	57.5% energy efficiency, 46.3% CO_2 reduction
11	Salimi et al. [61]	Environmental impact of CCHP	Various	CCHP reduces emissions, LCA confirms renewable advantage
12	Haghghi et al. [62]	Solar-driven CCHP in Iran	PTSC + ORC + Absorption Chillers	98% energy efficiency, validated with real data

13	Saini et al. [63]	Compact solar CCHP	ETC + ORC + ERC	3.16% exergy efficiency, 13 tons/year CO_2 savings
14	Wang et al. [64]	New CCHP with methanol storage	SOFC + ORC + AR/HP	96.96% energy efficiency, fuel savings by 19.1%
15	Zhao et al. [65]	ORC-based CCHP configuration comparison	PTC + Absorption Chiller	Sequential system best efficiency (45.82%)
16	Xia et al. [66]	Solar DHC system optimization	TCHP + ETC + PV	43.56% UEC reduction compared to benchmark
17	Zarei et al. [67]	Series PVT–PTC system	Regenerative ORC + VCRC	6.4 years payback, 75.6% energy efficiency
18	Li et al. [68]	Community solar CCHP with DSM	PV, Storage, DSM	8.7% exergy efficiency improvement
19	Bataineh [32]	Solar Stirling CCHP systems	Dish Stirling + Hybrid backup	Up to 96% system efficiency
20	Huang et al. [69]	Energy storage in renewable CCHP	BAT, TES, HS storage systems	Best results: BAT+HS+TES combo at 100% SSR
21	Nami et al. [70]	Solar–biomass CCHP plant	Externally fired GT + CPVT	82.1% overall efficiency, optimized for winter
22	Wu et al. [33]	Solar thermochemical hybrid CCHP	ICE + Solar-driven syngas	71.55% CO_2 reduction in Harbin case
23	Behzadi et al. [71]	Solar cogeneration system with DH	PVT + ULTDH/LTDH/3GDH	Highest efficiency with ULTDH (70%)
24	Borhani et al. [72]	Regional performance of solar CCHP	ANN prediction + PVT	ANN R^2 up to 0.999, fastest in warm climates
25	Herrando et al. [73]	PVT-based S-CCHP system	PVT + Hot Water Storage + Chiller	16.7-year payback; highest sustainability
26	García-Domínguez et al. [74]	Solar CCHP with advanced exergy method	Superheated ORC + H_2O/LiBr AHP	152.4% energy efficiency, PTC major loss point

27	Chen et al. [75]	Solar CCHP for building energy supply	Superheated ORC + AHP	84.9% ORC exergy efficiency
28	Aieneh et al. [76]	Standalone solar CCHP with hydrogen	Supercritical CO_2 + ERC + PEM	Net power 11.7 MW, hydrogen 12.95 g/s

This chapter highlighted the significant advancements and various approaches adopted globally in the development of solar-driven combined cooling, heating, and power (CCHP) systems. While previous research has shown impressive improvements in system configurations, energy efficiency, and environmental benefits, most studies focus either on specific climates, technologies, or conventional hybrid systems without fully addressing integration under Libya's unique climatic, economic, and infrastructural conditions. Importantly, few works have systematically evaluated the application of regenerative Brayton cycles combined with absorption refrigeration and solar concentration technologies customized for regions with extremely high solar irradiation and critical energy shortages, such as Libya. Therefore, this thesis seeks to bridge this gap by designing, modeling, and analyzing a solar-driven CCHP system specifically tailored for Libya. It offers a novel and practical contribution by integrating advanced thermodynamic modeling with real local environmental conditions, aiming to enhance energy efficiency, reduce reliance on fossil fuels, and promote sustainable development in the region.

CHAPTER 3

SOLUTION METHODOLOGY

This chapter outlines the methodology used to design, model, and evaluate the performance of a proposed combined cooling, heating, and power (CCHP) system specifically designed for Libyan conditions. It begins by presenting the general system configuration and the rationale for selecting its main components and working fluids. A detailed thermodynamic model is then developed based on the principles of energy and thermal stress analysis. The chapter describes the simulation tools used to analyze the system behavior under realistic operational scenarios. Furthermore, the chapter identifies the assumptions used during the system design. Finally, the methodology for validating the developed model is discussed.

3.1. SYSTEM OVERVIEW AND CONCEPTUAL DESIGN

Figure 3.1 illustrates a Solar-Driven Combined Cooling, Heating, and Power (CCHP) System implemented in Libya, designed to optimize the use of solar energy for multiple energy needs—electric power, heating, and cooling. The system consists of a heliostat field and solar receiver, Brayton cycle (power generation loop), heating System, and cooling System (Absorption Refrigeration Cycle). The trigeneration system (CCHP) in this design efficiently utilizes solar energy to produce power, heating, and cooling simultaneously. Electrical power is generated by the turbine, which is driven by high-temperature air heated through concentrated solar energy. The system also recovers waste heat from the turbine exhaust to supply hot water through a dedicated heater, fulfilling heating demands. Additionally, the recovered thermal energy powers an absorption cooling system, which uses a lithium bromide-water solution to provide cooling. This integrated approach maximizes energy utilization and is particularly well-suited for regions with abundant solar resources like Libya.

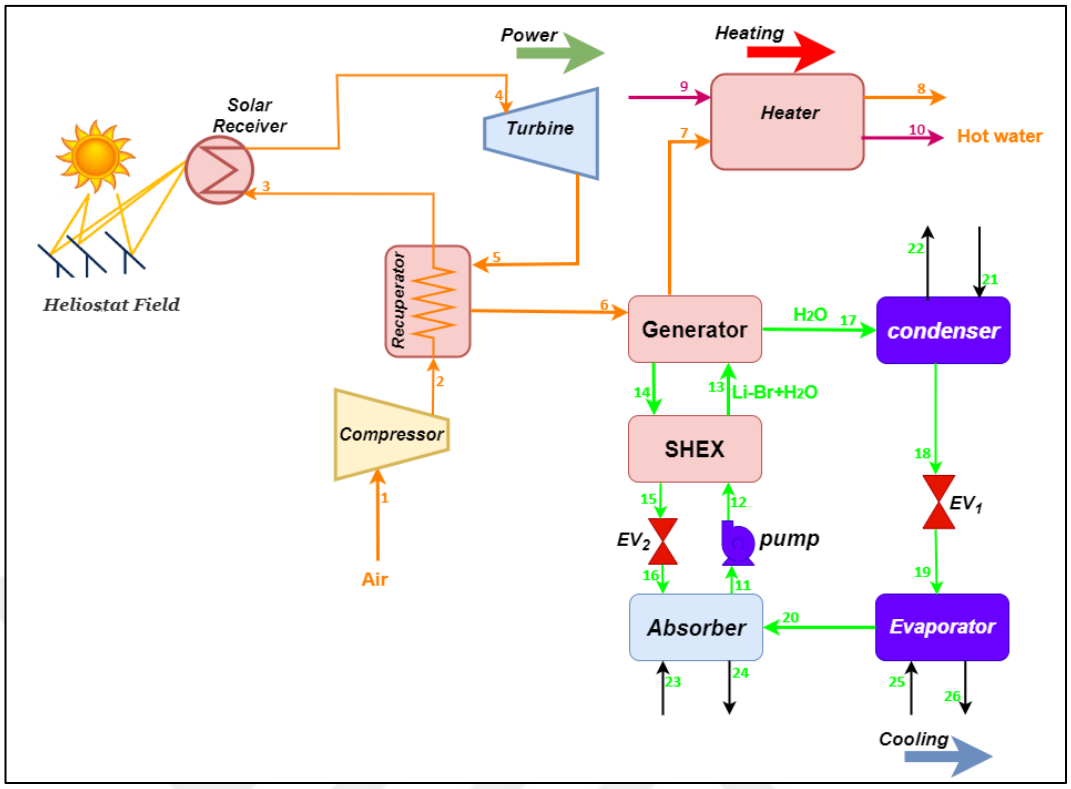

Figure 3. 1. Solar-driven combined cooling, heating, and power system in Libya.

3.1.1. Main Components and Flow Path

3.1.1.1. Heliostat Field and Solar Receiver

The heliostat field reflects and concentrates solar radiation onto the solar receiver, which collects high-temperature thermal energy.

The solar receiver heats the working fluid (likely air or another gas) that flows into the turbine.

3.1.1.2. Brayton Cycle (Power Generation Loop)

- Compressor (1 → 2): Ambient air is compressed, increasing its pressure and temperature.
- Recuperator (2 → 3): Pre-heats the compressed air using exhaust gases (enhances efficiency).

- Solar Receiver (3 → 4): Heats the air further using concentrated solar energy.
- Turbine (4 → 5): The hot air expands in the turbine, generating mechanical energy → converted to electricity.
- Recuperator (5 → 6): Transfers heat from turbine exhaust to incoming compressed air.
- Generator Heat Recovery (6 → 7): The exhaust heat is directed to the absorption cycle generator.

3.1.1.3. Heating System

- Heater (7 → 10): Uses part of the turbine exhaust heat to produce hot water for heating purposes.

3.1.1.4. Cooling System (Absorption Refrigeration Cycle)

This part of the system is a LiBr-H_2O absorption cycle, used to produce cooling energy. Key Components:

- Generator (7 → 13): Uses recovered heat to separate the refrigerant (water vapor) from the absorbent (LiBr).
- SHEX – Solution Heat Exchanger (13 ↔ 14, 12 ↔ 15): Enhances the thermal efficiency of the absorption cycle by exchanging heat between rich and weak LiBr solutions.
- Pump (11): Circulates the absorbent solution through the system.
- EV2 (15 → 16): Expansion valve for pressure control before the absorber.
- Absorber (16 → 24): Absorbs water vapor back into the LiBr solution, releasing heat in the process.
- Evaporator (19 → 25): Cools water by evaporating refrigerant under low pressure.
- EV1 (18 → 19): Expansion valve for refrigerant entering the evaporator.
- Condenser (17 → 21): Condenses the water vapor coming from the generator to liquid before entering EV1.

3.1.2. Selection of System Components and Working Fluids

The selection of system components and working fluids plays a crucial role in determining the efficiency, reliability, and overall performance of the solar-driven CCHP system. The harsh climatic conditions of Libya, characterized by high solar irradiation and significant cooling and heating demands, necessitate careful consideration of each element to ensure optimal operation throughout the year.

To harness the abundant solar resource effectively, a parabolic trough collector (PTC) system is selected as the primary solar concentrator. PTCs offer high optical efficiency and are suitable for generating medium-to-high-temperature heat required for driving thermodynamic cycles. The PTCs are designed to operate at temperatures ranging between 150°C and 400°C, which matches the needs of the regenerative Brayton cycle and absorption chiller integrated within the system.

For power generation, a regenerative Brayton cycle is employed. This cycle is favored for its high thermal efficiency, compact design, and suitability for decentralized energy production in remote areas. A recuperator is included to preheat the compressed air before combustion, thus enhancing cycle efficiency and reducing fuel consumption.

The cooling load is addressed by integrating a single-effect absorption chiller driven by the waste heat recovered from the Brayton cycle. Lithium bromide (LiBr)/water is selected as the working pair due to its high coefficient of performance (COP) and environmental friendliness. For heating purposes, the system utilizes direct thermal energy recovered from the Brayton cycle exhaust gases and supplementary solar heat.

The selection of each component and fluid was guided by key criteria, including:

- Compatibility with Libyan climatic conditions
- High thermal and exergetic efficiency
- Cost-effectiveness and availability
- Low environmental impact

- Operational reliability and ease of maintenance.

3.2. THERMODYNAMIC MODELING AND GOVERNING EQUATIONS

To accurately predict the performance of the proposed solar-driven CCHP system, a comprehensive thermodynamic model was developed. This model integrates the energy and exergy balances of each subsystem, ensuring a consistent and detailed evaluation of system behavior under varying operating conditions.

3.2.1. Assumptions

The following assumptions were made to simplify the modeling process without significantly compromising the accuracy:

- Steady-state and steady-flow conditions are assumed for all components.
- Pressure and heat losses in pipes and ducts are neglected.
- The solar collectors operate under uniform solar irradiation.
- The air in the Brayton cycle behaves as an ideal gas with constant specific heats.
- Air is assumed to be composed of 79% N2 and 21% O2 on a volume basis.
- The efficiency of auxiliary components, such as pumps and fans, is considered constant.
- The performance of the ARS is based on standard LiBr–water cycle behavior.
- In the ARS, the water leaving the evaporator and condenser is considered saturated vapor and saturated liquid, respectively.
- In the ARS, the LiBr–H_2O solution exiting the absorber and generator is assumed to be a saturated liquid and in thermodynamic equilibrium at the specified pressure and temperature conditions.
- Ambient temperature and pressure are used as reference conditions for the exergy analysis.

3.2.2. Energy Balance Equations

In this subsection, the equations used to model the system's energy and exergy aspects are presented and explained.

Mass balance equation:

$$\sum \dot{m}_i = \sum \dot{m}_e \quad (3\text{-}1)$$

The First Law of Thermodynamics (energy conservation) is applied to each component.

For a general control volume, the energy balance is expressed as [78,79]

$$\dot{Q} + \sum \dot{m}_i h_{\mathrm{i}} = \dot{W} + \sum \dot{m}_e h_e \quad (3\text{-}2)$$

where:

i = control volume inlet
e= control volume exit
$\dot{m}$= mass flow rate
$\dot{Q}$= rate of heat
$\dot{W}$= work net
h= enthalpy

Each main component (compressor, turbine, recuperator, ARS, and heat exchangers) was modeled individually using specific energy balance equations suited to their operation. Table 3.1 outlines the energy balance equations for the components of the solar-driven CCHP plant. These formulations are essential for evaluating the energy performance and efficiency of the overall system.

Table 3. 1. Energy balance equations in the solar- powered CCHP plant

Component	**Energy Balance Equation**
AC	$\dot{W}_{AC} = \dot{m}_1 (h_2 - h_1)$
Rec	$\dot{m}_2 (h_3 - h_2) = \dot{m}_5 (h_5 - h_6)$
SR	$\dot{Q}_{SR} = \dot{m}_3 (h_4 - h_3)$
GT	$\dot{W}_{GT} = \dot{m}_4 (h_4 - h_5)$
Heater	$\dot{Q}_H = \dot{m}_7 (h_7 - h_8) = \dot{m}_9 (h_{10} - h_9)$
Gen	$\dot{Q}_{Gen} = \dot{m}_6 (h_6 - h_7) = \dot{m}_{17} h_{17} + \dot{m}_{14} h_{14} - \dot{m}_{13} h_{13}$
Cond	$\dot{Q}_{Cond} = \dot{m}_{17} (h_{17} - h_{18}) = \dot{m}_{22} (h_{22} - h_{21})$
Ev_1	$\dot{m}_{18} h_{18} = \dot{m}_{19} h_{19}$
Evap	$\dot{Q}_{Evap} = \dot{m}_{19} (h_{20} - h_{19}) = \dot{m}_{25} (h_{25} - h_{24})$
Abs	$\dot{Q}_{abs} = \dot{m}_{23} (h_{24} - h_{23}) = \dot{m}_{11} h_{11} - \dot{m}_{16} h_{16} - \dot{m}_{20} h_{20}$
Pump	$\dot{W}_P = \dot{m}_{11} (h_{12} - h_{11})$
SHEX	$\dot{m}_{12} (h_{13} - h_{12}) = \dot{m}_{14} (h_{14} - h_{15})$
Ev_2	$\dot{m}_{15} h_{15} = \dot{m}_{16} h_{16}$

3.2.3. Exergy Analysis

To account for the quality of energy transformations, an exergy analysis was performed based on the Second Law of Thermodynamics. The general exergy balance for a control volume is [80,81]:

$$\dot{E}x_{\mathrm{Q}} + \sum \dot{m}_{\mathrm{i}} ex_{\mathrm{i}} = \dot{E}x_w + \sum \dot{m}_{\mathrm{e}} ex_{\mathrm{e}} + \dot{E}x_{\mathrm{dest}} \qquad (3\text{-}3)$$

where:

$\dot{E}x_{\mathrm{Q}}$ = exergy relevant to heat transfer

$\dot{E}x_w$ = exergy relevant to power

$\dot{E}x_{\mathrm{dest}}$ = exergy destruction within each component

The stream exergy rate by heat, work, and physical exergy is determined using the following equations [82,83].

$$\dot{E}x_{\mathrm{Q}} = \left(1 - \frac{T_{\mathrm{o}}}{T_k}\right)\dot{Q}_k \tag{3.4}$$

$$\dot{E}x_w = \dot{W} \tag{3.5}$$

$$ex = (h - h_o) - T_o(s - s_0) \tag{3.6}$$

The subscript "0" denotes the ambient pressure and temperature conditions. Furthermore, the exergy efficiency, as defined in Eq. (7), is employed to accurately assess the efficiency of each component.

$$\Psi = \left(1 - \frac{\dot{E}x_{\mathrm{dest}}}{\dot{E}x_{\mathrm{f}}}\right) = \frac{\dot{E}x_{\mathrm{p}}}{\dot{E}x_{\mathrm{f}}} \tag{3.7}$$

where

Ψ = exergy efficiency.
$\dot{E}x_{\mathrm{f}}$ = exergy of fuel.
$\dot{E}x_{\mathrm{p}}$ = exergy of product.

Table 3.2 presents the exergy balance equations for various components of the solar-driven CCHP plant. Each equation accounts for the exergy destruction within the respective component, considering the exergy inputs, outputs, and any work or heat interactions.

Table 3. 2. Exergy balance equations in the solar - powered CCHP plant

Component	Exergy Balance Equation
AC	$\dot{E}x_{\text{dest,AC}} = \dot{E}x_1 - \dot{E}x_1 + \dot{W}_{AC}$
Rec	$\dot{E}x_{\text{dest,Rec}} = \dot{E}x_2 - \dot{E}x_3 + \dot{E}x_5 - \dot{E}x_6$
SR	$\dot{E}x_{\text{dest,AC}} = \dot{E}x_3 - \dot{E}x_4 + \dot{E}_{Q,Solar}$
GT	$\dot{E}x_{\text{dest,GT}} = \dot{E}x_4 - \dot{E}x_5 - \dot{W}_{GT}$
Heater	$\dot{E}x_{\text{dest,H}} = \dot{E}x_7 - \dot{E}x_8 + \dot{E}x_9 - \dot{E}x_{10}$
Gen	$\dot{E}x_{\text{dest,Gen}} = \dot{E}x_6 - \dot{E}x_7 + \dot{E}x_{13} - \dot{E}x_{14} - \dot{E}x_{17}$
Cond	$\dot{E}x_{\text{dest,Cond}} = \dot{E}x_{17} - \dot{E}x_{18} + \dot{E}x_{21} - \dot{E}x_{22}$
Ev_1	$\dot{E}x_{\text{dest},Ev_1} = \dot{E}x_{18} - \dot{E}x_{19}$
Evap	$\dot{E}x_{\text{dest,Evap}} = \dot{E}x_{19} - \dot{E}x_{20} + \dot{E}x_{25} - \dot{E}x_{26}$
Abs	$\dot{E}x_{\text{dest,Abs}} = \dot{E}x_{20} + \dot{E}x_{16} - \dot{E}x_{11} + \dot{E}x_{23} - \dot{E}x_{24}$
Pump	$\dot{E}x_{\text{dest,P}} = \dot{E}x_{11} - \dot{E}x_{12} + \dot{W}_P$
SHEX	$\dot{E}x_{\text{dest,SHEX}} = \dot{E}x_{12} - \dot{E}x_{13} + \dot{E}x_{14} - \dot{E}x_{15}$
Ev_2	$\dot{E}x_{\text{dest},Ev_2} = \dot{E}x_{15} - \dot{E}x_{16}$

3.2.4 Solar Collector Modeling

The inlet heat gain from the heliostat field is defined as follows [84]:

$$\dot{Q}_{solar} = \eta_{\text{field}} * A_a * DNI \tag{3-8}$$

Where:

$\dot{Q}_{solar}$ = heat gain from the heliostat field

A_h= collector aperture area (m^2)

η_{field}= optical efficiency

DNI= direct normal irradiance

Useful heat transfer rate for the solar receiver is computed from:

$$\dot{Q}_{\text{Solar}} = \dot{m}_3\left(h_{rec,out} - h_{rec,in}\right) \quad (3\text{-}9)$$

3.3. INPUT PARAMETERS TO THE SOLAR-DRIVEN CCHP SYSTEM

Table 3.3 summarizes the key input values used in the design and simulation of a solar-powered CCHP system. The heliostat field parameters, including a total reflective area of 40,000 square meters in Tripoli, Libya, were selected to match the local solar resource (DNI = 800 W/m²) as reported by NASA. These inputs form the basis for accurately modeling and analyzing the performance of the integrated CCHP system under realistic environmental conditions.

Table 3. 3. Input values utilized for the design of the solar-powered CCHP model.

Component	Parameter	Value
Regenerative Brayton cycle	Pressure ratio	8
	Compressor's inlet temperature	30℃
	Compressor's inlet pressure	100 kPa
	Compressor's isentropic efficiency	81%
	Air flow rate	40 kg/s
	Turbine's isentropic efficiency	88%
	Regenerative effectiveness	70%
Heliostats field	Area	50000 m^2
	Location	Tripoli- Libya
	Latitude	32.8874° N
	Longitude	13.1873° E
	DNI	800 W/m^2
ARS	Condenser temperature (T_{18})	39 ℃
	Generator temperature (T_{14})	88 ℃
	Absorber temperature (T_{11})	37 ℃
	SHEX effectiveness	55 (%)
	Evaporator temperature (T_{19})	7 ℃
	LiBr Solution strength (%)	53 (%)

3.4. SIMULATION TOOLS AND SOFTWARE UTILIZED

To perform the thermodynamic modeling, simulation, and analysis of the proposed solar-driven CCHP system, the Engineering Equation Solver (EES) software was employed. EES was selected over other tools due to its accurate and extensive thermodynamic property databases, ease of solving complex coupled equations, capability to perform optimization and parametric analysis, and rapid computation times, enabling efficient exploration of multiple operating scenarios.

The simulation process involved the following steps:

- Defining all input parameters, including solar irradiation data, ambient conditions, mass flow rates, pressures, and temperatures at various system points.
- Implementing the energy balance and exergy balance equations for each component.
- Utilizing EES's iterative solving capabilities to achieve convergence for all unknown variables.
- Conducting parametric studies to investigate the effects of varying design parameters such as the pressure ratio in the Brayton cycle, solar collector area, and cooling load demands.
- Calculating key performance indicators, including thermal efficiency, exergy efficiency, heat transfer rates, power outputs, and system losses.

3.5. PERFORMANCE EVALUATION CRITERIA

In order to comprehensively assess the behavior and efficiency of the proposed hybrid solar-driven Brayton system, several performance evaluation criteria were employed. These criteria enable a multi-dimensional understanding of both the thermodynamic and economic aspects of the system. The following parameters were calculated and analyzed:

3.5.1. Net Power Output

Net power output is the difference between the total power generated by the turbine(s) and the power consumed by system auxiliaries, such as compressors and pumps. It serves as a primary indicator of the system's ability to meet electrical demand. The power output from the solar-derived CCHP plant can be found thus [85]:

$$\dot{W}_{\text{net}} = \dot{W}_{\text{GT}} - \dot{W}_{\text{AC}} + \dot{W}_{ST} - \dot{W}_{\text{P}} \quad (3\text{-}10)$$

3.5.2. Thermal Energy Outputs:

- Heating Energy Output: Calculated based on the amount of heat recovered for heating purposes, typically from the Brayton cycle recuperator or condenser stages.
- Cooling Energy Output: Assessed through the performance of the absorption or ORC cooling subsystem using chilled water production.

The heating and cooling loads obtained from the solar-driven CCHP plant are given as follows:

$$\dot{Q}_{\text{heating}} = \dot{Q}_{\text{H}} \quad (3\text{-}11)$$

$$\dot{Q}_{\text{cooling}} = \dot{Q}_{\text{Evap}} \quad (3\text{-}12)$$

3.5.3. Energy Efficiency

Energy efficiency represents the ratio of useful energy output (power generation, heating, or cooling) to the total energy input received by the system. The electrical energy efficiency and overall energy efficiency of the CCHP system are calculated from the following equations:

$$\eta_{\text{I,electrical}} = \frac{\dot{W}_{\text{net}}}{\dot{Q}_{solar}} \tag{3-13}$$

$$\eta_{\text{I,CCHP}} = \frac{\dot{W}_{\text{net}} + \dot{Q}_{\text{heating}} + \dot{Q}_{\text{cooling}}}{\dot{Q}_{solar}} \tag{3-13}$$

3.5.4. Exergy Efficiency

Exergy efficiency evaluates the system's ability to convert available energy into useful work, considering the quality of energy. The electrical exergy efficiency and overall exergy efficiency of the CCHP system are calculated from the following equations:

$$\eta_{\text{II,electrical}} = \frac{\dot{W}_{\text{net}} + \dot{Q}_{\text{heating}} + \dot{Q}_{\text{cooling}}}{\dot{\text{E}}x_{\text{Q}_{\text{solar}}}} \tag{3-14}$$

$$\eta_{\text{II,CCHP}} = \frac{\dot{W}_{\text{net}}}{\dot{\text{E}}x_{\text{Q}_{\text{solar}}}} \tag{3-15}$$

3.5.5. Coefficient of Performance of ARS

The Coefficient of Performance (COP) of the absorption refrigeration system is a critical indicator used to evaluate the cooling efficiency of the integrated CCHP system. It is defined as the ratio of the useful cooling output to the thermal energy input required to drive the absorption process. The COP is calculated by [86]:

$$COP = \frac{\dot{Q}_{\text{Evap}}}{\dot{Q}_{\text{G}} + \dot{W}_{\text{P}}} \tag{3-16}$$

3.5. VALIDATION OF THE THERMODYNAMIC MODEL

The validation was conducted only for the ARS system, as no comparable model for the solar regenerative Brayton cycle was found in the literature. Table 3.4 shows the validation process of the absorption refrigeration (ARC) system model using the data

reported by Ren et al. [87]. In this study, the same input values used in the reference study were entered into the current model, with the aim of focusing only on comparing the outputs between the two models without making any modifications to the basic operating conditions. The output results showed excellent agreement between the reference study and the current study, with very small relative differences. The relative difference in the heat entering the $\dot{Q}_{\text{Gen}}$ was only 0.02%, while the differences in the heat removed from the $\dot{Q}_{\text{Abs}}$, $\dot{Q}_{\text{Cond}}$, and $\dot{Q}_{\text{Evap}}$ were 0.006%, 0.083%, and 0.072%, respectively. The relative difference in the coefficient of performance (COP) was 0.013%, reflecting the current model's high accuracy in representing system performance.

Table 3. 4. Model validation for the ARC system using the data reported by Ren et al. [87]

Parameter	Literature study	Present study	Relative error (%)
Input parameter			
Generator temperature	87.8°C	87.8°C	-
Absorber temperature	37.8 °C	37.8 °C	-
SHEX effectiveness	0.7	0.7	-
Evaporator temperature	7.2 °C	7.2 °C	-
Mass of refrigerant	1 kg/s	1 kg/s	-
Output parameter			
$\dot{Q}_{\text{Gen}}$	3074.6 kW	3075.1 kW	0.02
$\dot{Q}_{\text{Abs}}$	2946 kW	2946.2 kW	0.006
$\dot{Q}_{\text{Cond}}$	2504.2	2506.3 kW	0.083
$\dot{Q}_{\text{Evap}}$	2354.1	2355.8 kW	0.072
COP	0.7663	0.7662	0.013

CHAPTER 4

RESULTS AND DISCUSSION

This chapter presents the results obtained from the thermodynamic modeling and simulation of the solar-powered CCHP system. The system's performance is evaluated through detailed analysis of thermodynamic properties at different operational states, overall energy and exergy efficiencies, and component-level exergy destruction rates. Key performance indicators, such as net power output, heating load, cooling load, and coefficients of performance, are discussed comprehensively. In addition, the impact of varying system parameters, particularly the pressure ratio, on the overall system behavior is investigated. The findings provide insights into the strengths and limitations of the proposed system and highlight opportunities for enhancing its thermodynamic performance under Libyan climatic conditions.

4.1. THERMODYNAMIC PROPERTIES AT KEY SYSTEM STATES

Table 4.1 presents the thermodynamic properties at various states for the solar-powered CCHP system. The data include mass flow rate, pressure, temperature, enthalpy, and specific enthalpy values at different operational points within the system. The enthalpy and entropy values are provided to support detailed energy balance and performance analysis of the solar-driven system.

Table 4. 1. Thermodynamic properties at different states for the solar-powered CCHP system

Mass (kg/s)	Pressure (bar)	Temperature (°C)	Enthalpy (kJ/kg)	Enthalpy (kJ/kg · K)
40	1	30	303.6	5.716
40	8	327.8	608.4	5.817
40	8	567.8	867.5	6.18
40	8	1192	1594	6.823
40	1	677.1	989.9	6.913
40	1	435.4	722.8	6.589
40	1	235.4	512.2	6.24
40	1	100	374.1	5.925
26.41	1	25	104.9	0.3672
26.41	1	75	314.1	1.016
19.98	0.008634	37	82.23	0.239
19.98	0.06944	37.15	82.23	0.239
19.98	0.06944	69.87	151.8	0.4519
17.08	0.06944	88	219.9	0.4824
17.08	0.06944	60.03	167.5	0.3313
17.08	0.008634	48.41	167.5	0.3314
2.9	0.07	88	2656	7.504
2.9	0.07	39	163.4	0.559
2.9	0.01002	7	163.4	0.5844
2.9	0.01002	7	2514	8.974
173	1	30	125.8	0.4367
173	1	40	167.6	0.5724
407.1	1	30	125.8	0.4367
407.1	1	35	146.7	0.5051
108.6	1	30	125.8	0.4367
108.6	1	15	63.08	0.2244

4.2. OVERALL SYSTEM PERFORMANCE RESULTS

Table 4.2 summarizes key energy and exergy performance indicators for the solar-powered CCHP system. The system achieves a net power output of 11,987 kW, alongside a heating load of 5,523 kW and a cooling load of 6,816 kW, illustrating its capability to simultaneously deliver electricity, heat, and cooling demands efficiently. CCHP energy efficiency is recorded at 83.67%. However, the CCHP exergy efficiency is lower at 45.59%. For the electrical performance, the electrical energy efficiency reaches 41.23%, while the electrical exergy efficiency slightly exceeds it at 43.42%. Finally, the coefficient of performance (COP) of the integrated absorption refrigeration system (ARS) is reported as 0.81.

Table 4. 2. Energy and Exergy Performance of solar-powered CCHP system

Aspect	Symbol	Value
Net power output (kW)	$\dot{W}_{net}$	11987
Heating load (kW)	$\dot{Q}_{heating}$	5523
Cooling Load (kW)	$\dot{Q}_{cooling}$	6816
CCHP energy efficiency (%)	$\eta_{I,CCHP}$	83.67
CCHP exergy efficiency (%)	$\eta_{II,CCHP}$	45.59
Electrical energy efficiency (%)	$\eta_{I,electrical}$	41.23
Electrical exergy efficiency (%)	$\eta_{II,electrical}$	43.42
Coefficient of Performance of ARS	COP	0.81

4.3. EXERGY DESTRUCTION ANALYSIS OF SYSTEM COMPONENTS

Table 4.3 provides the exergy analysis for each component of the solar-powered CCHP system. The table lists the exergy destruction (in MW and percentage) and the corresponding exergy efficiency for each system component. The total exergy destruction in the system is 16.88 MW, distributed among the different components.

The solar receiver (SR) is responsible for the highest share of exergy destruction, accounting for 45.33% of the total, significantly affecting the system's overall exergy performance. This component also shows a moderate exergy efficiency level of 73.55%. The generator and heater are the next largest contributors to exergy destruction, at 12.98% and 8.147% respectively. The generator's relatively low exergy efficiency of 47.8% and the heater's very low efficiency of 19.35%. The air compressor (AC), recuperator (Rec), and gas turbine (GT) show much better performance, with low percentages of exergy destruction (7.254%, 4.633%, and 6.48%, respectively) and high exergy efficiencies (89.97%, 88.42%, and 95.67%, respectively). The gas turbine has the highest efficiency among the main power-generating components. For the ARS, components such as the condenser, evaporator, and absorption unit show varying exergy efficiencies. The evaporator achieves a reasonable exergy efficiency of 63.89%, while the condenser and absorber demonstrate much poorer performances, particularly the absorber with only 6.74% efficiency.

Table 4. 3. Exergy analysis for each component of the solar-powered CCHP system

Component	$\dot{E}_{destruction}$ **(MW)**	$\dot{E}_{destruction}$ **(%)**	**Exergy efficiency (%)**
AC	1.224	7.254	89.97
Rec	0.7822	4.633	88.42
SR	7.653	45.33	73.55
GT	1.094	6.48	95.67
Heater	1.375	8.147	19.35
Gen	2.192	12.98	47.8
Cond	1.007	5.964	10.67
Ev_1	0.022	0.13	36.88
Evap	0.4386	2.598	63.89
Abs	1.08	6.4	6.74
Pump	0	0	100

SHEX	0.0123	0.073	89.1
Ev_2	0.0005	0.003	84.52
Total	16.88	100	-

4.4. PARAMETRIC ANALYSIS

In this section, a parametric analysis is conducted to investigate the effect of varying key operating parameters on the performance of the solar-powered CCHP system.

Figure 1 illustrates the relationship between the pressure ratio and three key performance parameters of the solar-driven CCHP system: Net power output, cooling load, and heating load. The findings showed that the net power output increases significantly with the pressure ratio. In a solar-driven Brayton cycle, higher pressure ratios maximize the utility of solar heat supplied to the system. The working fluid reaches a higher temperature and pressure, leading to a more efficient conversion of solar thermal energy into shaft power. At higher pressure ratios, the turbine inlet temperature remains high, and the turbine exit pressure decreases relative to the inlet. This increases the enthalpy drop across the turbine, meaning more energy is extracted and converted to power. Although compressor work also increases with pressure ratio, the gain in turbine output power is greater than the additional work required by the compressor. The net result is a significant increase in the net power output (turbine work – compressor work). The net power output starts at approximately 10,800 kW at a pressure ratio of 6, rising to nearly 13,500 kW at a pressure ratio of 12. This increase reflects the improved thermodynamic efficiency of the Brayton cycle with higher pressure ratios, leading to better energy conversion. The cooling load also shows a modest but steady increase from about 6775 kW to 6885 kW. This indicates enhanced thermal energy available for the absorption cooling process due to increased turbine exhaust heat at higher pressure ratios. The heating load mirrors the cooling load's behavior with a similar trend and slightly higher values. It rises from approximately 6785 kW to 6890 kW, confirming that recovered heat becomes more substantial and usable for heating applications at elevated pressure ratios. These results show that operating the system at higher pressure ratios (10–12) is most beneficial for

maximizing total energy output (trigeneration) without compromising the cooling/heating balance.

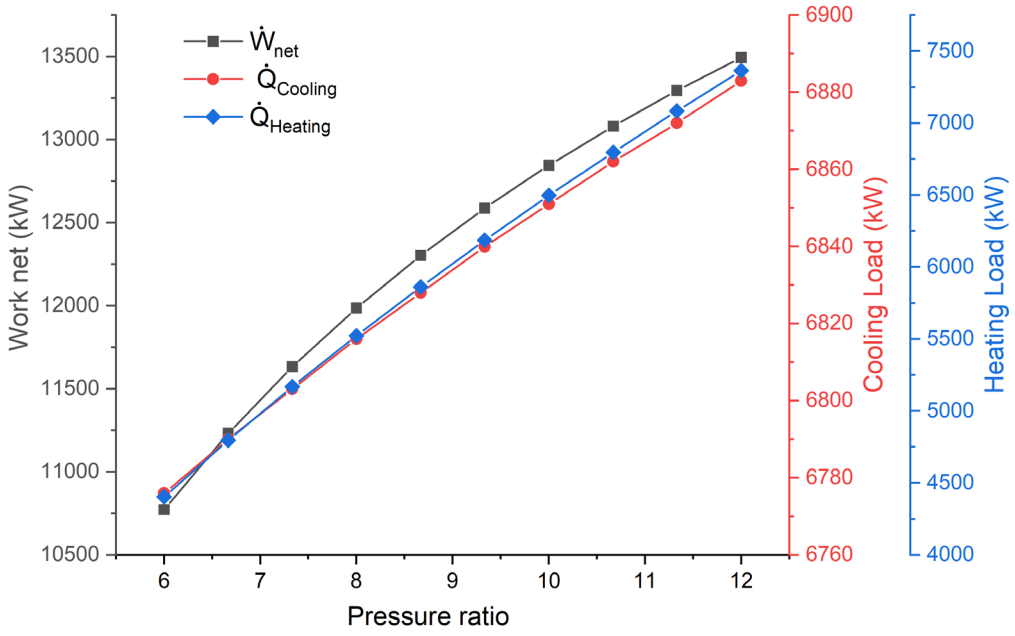

Figure 4. 1. Effect of pressure ratio on net power output, cooling load, and heating load in a solar-driven CCHP system.

Figure 2 shows how the pressure ratio affects the performance of a solar-driven CCHP system, by tracking five key indicators: electrical energy and exergy efficiencies, overall energy and exergy efficiencies of the CCHP system, and coefficient of performance of the Absorption Refrigeration Cycle. The results show that increasing the pressure ratio from 6 to 12 substantially improves the system's performance. The energy efficiency increases from 81.2% to 90.9%, while the electrical exergy efficiency improves from 57.4% to 71.7%. However, when second-law analysis is applied to the overall CCHP system, the efficiency increase is more modest, highlighting the impact of exergy degradation in heating and cooling processes. These results underscore the value of high-pressure ratios for improving the performance of solar-driven CCHP systems, particularly in regions like Libya with strong solar potential. Electrical Energy Efficiency ($\eta_{I,electrical}$) increases consistently with the pressure ratio. At PR = 6, the value is approximately 39%, while at PR = 12, it reaches around 49%, marking a 10 %point gain. This improvement is primarily due to the enhanced thermodynamic performance of the Brayton cycle. As the pressure ratio

increases, the expansion process in the turbine becomes more effective, leading to greater net power output while the solar input remains nearly constant. Electrical Exergy Efficiency ($\eta_{II,electrical}$) also rises with the pressure ratio, starting at around 37% for PR = 6 and increasing to about 47% at PR = 12. Although this is slightly lower than the first-law electrical efficiency at all points, the trend is similar. The difference between $\eta_{I,electrical}$ and $\eta_{II,\,electrical}$ reflects real-world irreversibilities, especially in the turbine, heat exchangers, and recuperator. Nevertheless, the increase in $\eta_{II,electrical}$ with PR shows reduced exergy destruction as operating conditions improve. The CCHP System Energy Efficiency ($\eta_{I,CCHP}$), which includes electrical output, heating, and cooling, also improves from about 87% at PR = 6 to 96% at PR = 12. This high efficiency reflects effective utilization of waste heat for heating and cooling, in addition to power generation. The increase with PR is largely attributed to the boost in turbine output, which supplements the heat recovery process. Unlike the CCHP energy efficiency, the CCHP exergy efficiency ($\eta_{II,CCHP}$) shows more moderate growth—from approximately 53% at PR = 6 to around 73% at PR = 12. This is expected because, while all energy forms (electrical, heating, and cooling) are included in energy efficiency, exergy efficiency accounts for the quality of energy. Heating energy, especially at low temperatures, contributes less exergy due to its proximity to ambient temperature. Interestingly, COP_ARC remains nearly constant at about 0.84 across the entire range of pressure ratios. This suggests that the absorption cooling subsystem is not significantly influenced by the Brayton cycle pressure ratio. The ARC performance depends more on generator and absorber temperature levels rather than turbine operational characteristics, which confirms that cooling performance is decoupled from pressure ratio changes.

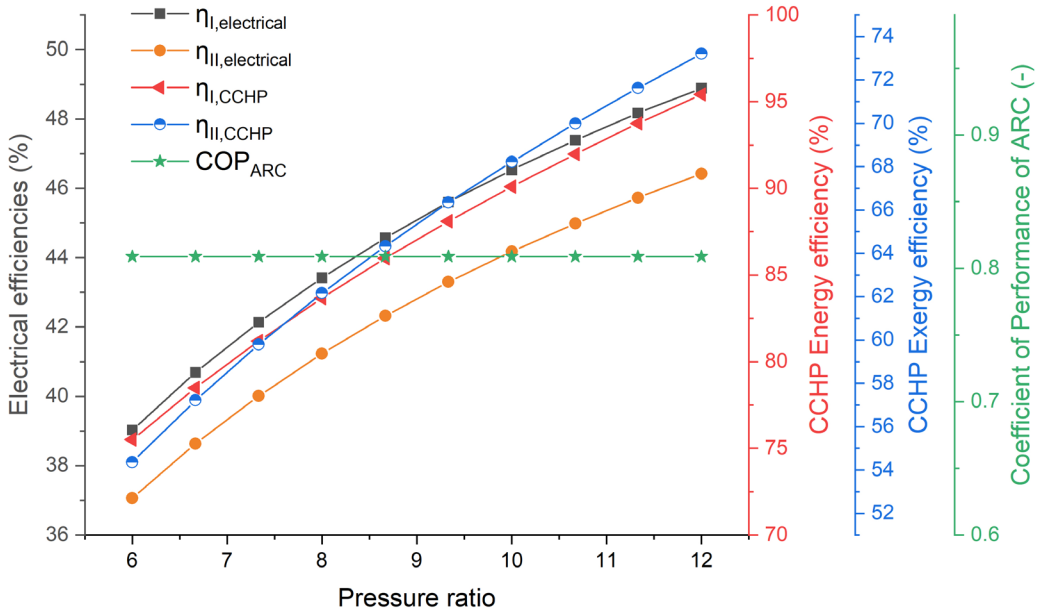

Figure 4. 2. Variation of electrical, energy, and exergy efficiencies of the CCHP system and COP of the absorption refrigeration cycle with pressure ratio.

Figure 3 presents the variation in three key outputs: the net power output ($\dot{W}_{net}$), cooling load ($\dot{Q}_{cooling}$), and heating load ($\dot{Q}_{heating}$) as a function of compressor isentropic efficiency, ranging from 0.70 to 0.88. The analysis emphasizes the importance of selecting a high-efficiency compressor in solar-driven Brayton-based CCHP systems. It boosts net power significantly while only marginally affecting the thermal output, making it ideal for applications prioritizing electrical generation without severely compromising on heating or cooling capabilities. The net power output increases from approximately 10,750 kW at a compressor efficiency of 0.70 to about 13,250 kW at an efficiency of 0.88. This positive correlation can be attributed to reduced compressor work as isentropic efficiency improves. In a solar-driven Brayton cycle, this leads to improved overall cycle performance and higher electrical output. As compressor efficiency increases, the cooling load decreases gradually from around 6885 kW to 6778 kW. This is due to the lower exhaust temperature from the turbine with reduced heat losses, which reduces the thermal energy available to drive the generator. In other words, when more power is extracted mechanically, less waste heat is available for the absorption cooling system, slightly lowering the cooling capacity. Similarly, the heating load decreases from approximately 6888 kW at 0.70 efficiency to about 6775 kW at 0.88. Like the cooling subsystem, the heating system depends on

recovered thermal energy from turbine exhaust. As less heat is lost (and more is converted into mechanical work), less residual heat is available for heating water, causing a slight decline in thermal recovery.

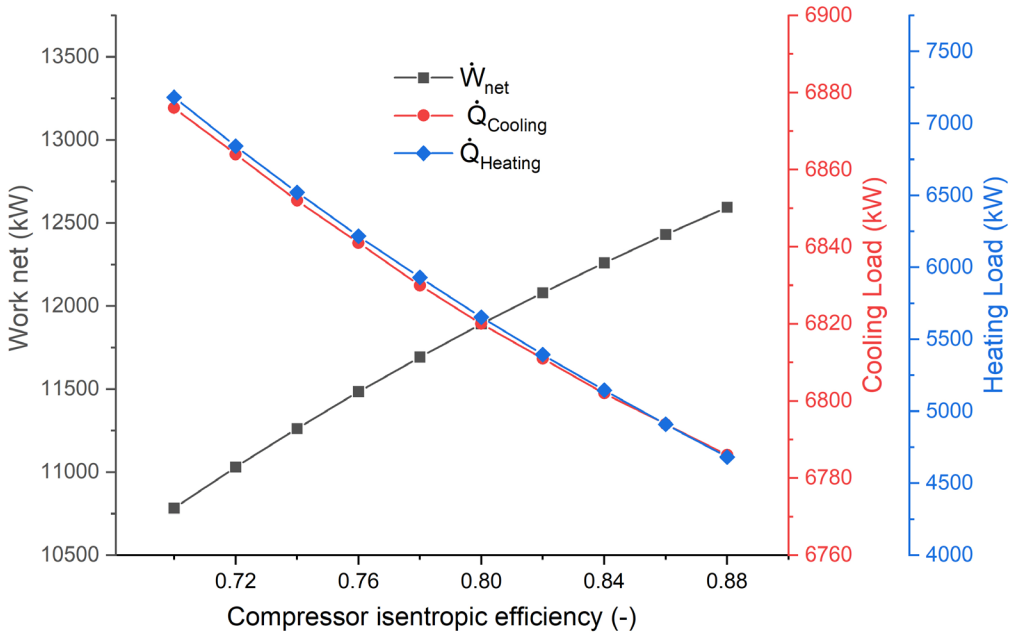

Figure 4. 3. Effect of compressor isentropic efficiency on net power output, cooling load, and heating load in a solar-driven CCHP system.

Figure 4 shows how variations in compressor isentropic efficiency (from 0.70 to 0.88) affect the efficiencies of the CCHP system. The results showed that while electrical efficiencies (energy and exergy) improve, CCHP energy and exergy efficiencies slightly decline, due to decreased availability of heat for secondary uses (heating/cooling). The ARC subsystem remains thermally isolated, showing a steady COP regardless of the Brayton cycle's internal performance. The electrical energy efficiency ($\eta_{I,electrical}$) increases significantly from about 39% at 0.70 efficiency to approximately 45.5% at 0.88. This is due to reduced compressor work as efficiency improves, which leads to a higher net work output from the Brayton cycle. The more efficient the compression, the less energy is wasted, increasing overall electrical energy conversion efficiency. The electrical exergy efficiency ($\eta_{II,electrical}$) also rises from around 37% to about 43% over the efficiency range. This reflects the increased electrical output and the improved utilization of high-quality (exergy-rich) solar input. Exergy efficiency is consistently lower than energy efficiency due to irreversibility

losses, but both improve with better compressor performance. The CCHP energy efficiency ($\eta_{I,CCHP}$) shows a slight downward trend, decreasing from 86% at low compressor efficiency to 83% at high efficiency. The decrease is due to less waste heat as compressor efficiency improves. As less energy is lost in the compression process, more of it is converted to electricity. However, this means less thermal energy is available for heating and cooling, slightly reducing the overall energy recovery. Also, CCHP Exergy Efficiency ($\eta_{II,CCHP}$) gradually decreases, from about 62% at low efficiency to 60% at high efficiency. This aligns with reduced thermal output quality due to lower waste heat. COP_{ARC} remains almost constant at 0.82 across all isentropic efficiency values. This stability indicates that the absorption refrigeration cycle's performance is independent of Brayton cycle compressor efficiency.

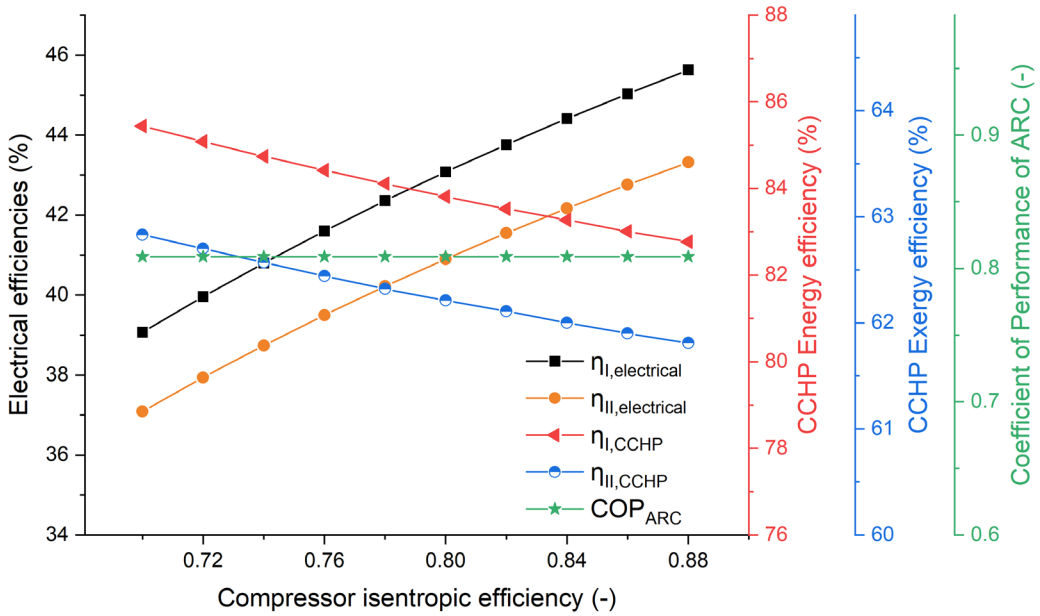

Figure 4. 4. Variation of electrical, energy, and exergy efficiencies of the CCHP system and COP of absorption refrigeration cycle with compressor isentropic efficiency.

Figure 5 shows how changes in turbine isentropic efficiency, ranging from 0.70 to 0.90, impact the following key outputs of the solar-driven CCHP system: net electrical power output, cooling load, and heating load. The results showed that improving turbine isentropic efficiency significantly enhances power production in solar-driven CCHP systems. Net power output is highly sensitive to turbine isentropic efficiency,

but the cooling and heating outputs decline modestly (~85 kW drop across the range), suggesting a trade-off between mechanical work and thermal recovery. Net power increases substantially with turbine efficiency. It rises from approximately 7,000 kW at 0.70 efficiency to over 12,500 kW at 0.90. This is expected because as the turbine's isentropic efficiency improves, more enthalpy is dropped across the turbine and converted into mechanical work, leading to higher electrical output. The turbine becomes more effective at extracting useful work from the hot, high-pressure air. The cooling load decreases slightly from about 6885 kW to 6805 kW. This is because less thermal energy remains in the turbine exhaust as more is converted into mechanical work. Since the absorption chillers depend on turbine exhaust heat (as the generator heat source), less available heat results in lower cooling capacity. Also, the heating load follows a similar downward trend to the cooling load, dropping from around 6895 kW to 6800 kW. This again reflects the reduced exhaust heat from the turbine at higher isentropic efficiencies. As more energy is extracted as useful power, less residual heat is available for space heating or hot water.

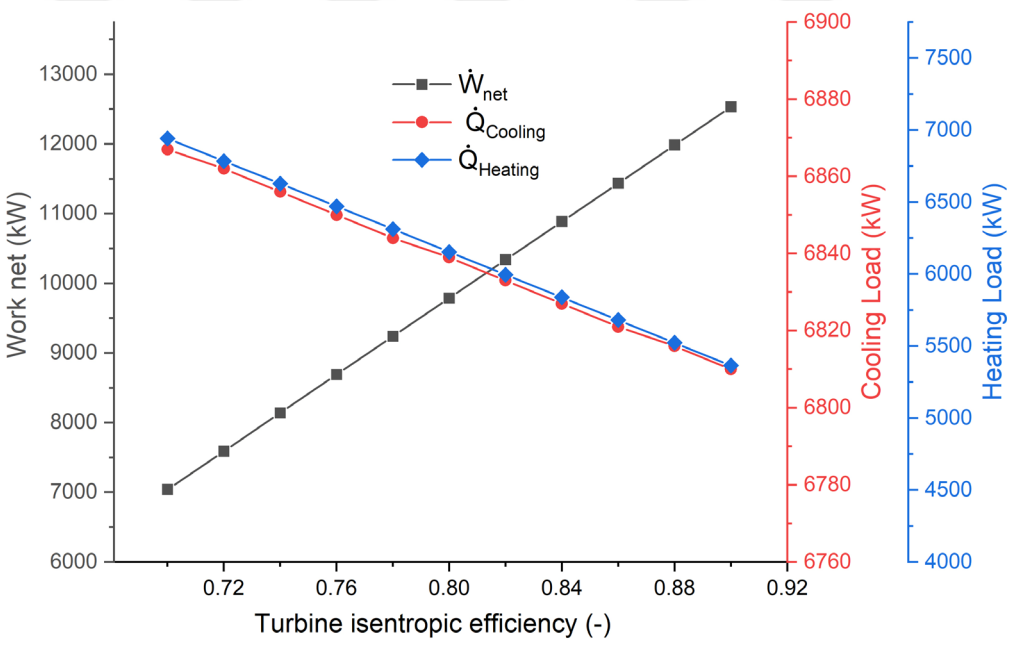

Figure 4. 5. Effect of turbine isentropic efficiency on net power output, cooling load, and heating load in a solar-driven CCHP system.

Figure 6 illustrates the impact of varying the turbine isentropic efficiency (ranging from 0.70 to 0.90) on the overall efficiencies of the CCHP system. The results revealed

that turbine isentropic efficiency significantly impacts all performance metrics, including electrical and overall system efficiency. All efficiency curves show a positive and nearly linear relationship, indicating improved thermodynamic behavior with higher turbine quality. Unlike compressor improvements, which may trade off heat recovery, the system performs better holistically with turbine optimization. COP of the ARC subsystem remains unaffected, confirming its thermal independence from turbine efficiency changes. Electrical energy efficiency rises from approximately 26% at 0.70 efficiency to nearly 45.5% at 0.90. The steep and linear increase indicates a direct gain in electrical output with higher turbine efficiency. As the isentropic efficiency of the turbine improves, it converts more of the available thermal energy into mechanical work. The electrical exergy efficiency similarly increases from ~24% to ~43%, paralleling the energy efficiency trend. It is consistently lower than energy efficiency, as it accounts for irreversibilities and low energy quality. This improvement suggests better use of high-quality (exergy-rich) solar energy at higher turbine efficiency. CCHP energy efficiency starts at around 22% at 0.70 and climbs steadily to about 41% at 0.90. This shows that electrical output and overall trigeneration performance improve as more energy is converted into useful work. CCHP exergy efficiency grew from ~23% to ~42%. It improves more slowly than energy efficiency due to the lower exergy content of thermal outputs (cooling and heating). Still, the upward trend confirms that the quality of overall system output improves as the turbine becomes more efficient. COP_{ARC} remains steady at around 0.83 for all values of turbine efficiency. This shows that the performance of the absorption cooling cycle is independent of the turbine isentropic efficiency.

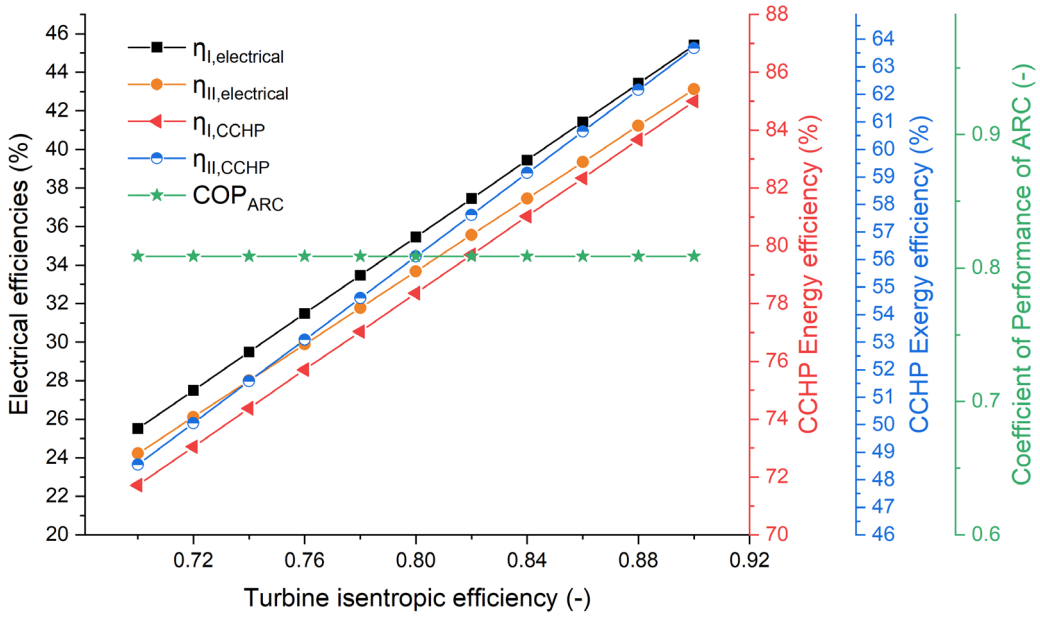

Figure 4. 6. Variation of electrical, energy, and exergy efficiencies of the CCHP system and COP of the absorption refrigeration cycle with turbine isentropic efficiency.

Figure 7 illustrates the effect of changes in recuperator effectiveness, ranging from 0.50 to 0.80, on key outputs of the solar-driven CCHP system: net electrical power output, cooling load, and heating load. The findings demonstrate that higher recuperator effectiveness enhances internal heat recovery and may improve overall cycle efficiency, reducing the thermal energy available for downstream heating and cooling uses. The cooling load drops gradually, reflecting reduced turbine exhaust heat input to the absorption cycle. The heating load drops significantly, making recuperator effectiveness a critical factor when heating is a system priority. The net power output remains relatively unchanged, fluctuating slightly around 12,000 kW throughout the range of recuperator effectiveness. This is because the recuperator is primarily a heat recovery device and does not directly impact the work-producing components (turbine or compressor). Its primary function is to preheat the compressed air before entering the solar receiver, reducing the need for external heat input—not affecting mechanical power generation significantly. The cooling load decreases from about 6940 kW at 0.50 effectiveness to about 6780 kW at 0.80 effectiveness. As recuperator effectiveness improves, more heat is recovered internally, which means less thermal energy is available in the turbine exhaust to drive the absorption cooling system. The

absorption cycle depends on this exhaust heat as the generator input; thus, a more effective recuperator reduces the waste heat reaching that point. The heating load shows the most significant drop, from around 13,350 kW to just below 10,000 kW. This sharp decrease is due to reduced exhaust gas temperature as more energy is internally recuperated to preheat the working fluid. Less high-temperature waste heat is available for water heating, directly impacting heating capacity.

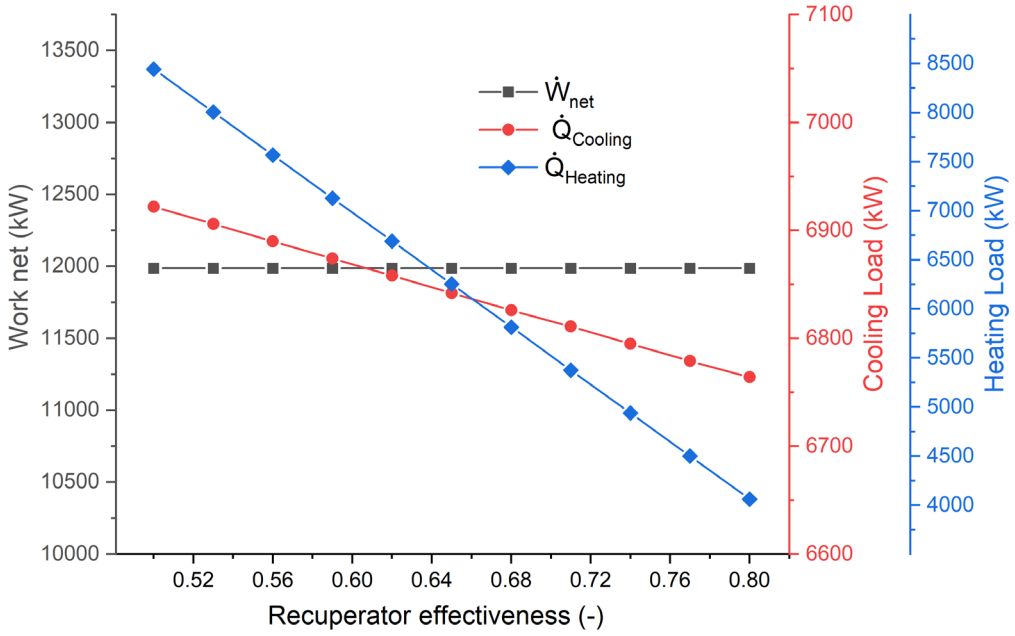

Figure 4. 7. Effect of recuperator effectiveness on net power output, cooling, and heating loads in a solar-driven CCHP system.

Figure 8 shows how varying recuperator effectiveness from 0.50 to 0.80 affects the following performance indicators: First-law electrical efficiency ($\eta_{I,electrical}$), Second-law electrical efficiency ($\eta_{II,electrical}$), CCHP energy efficiency ($\eta_{I,CCHP}$), CCHP exergy efficiency ($\eta_{II,CCHP}$), and Coefficient of performance of the absorption refrigeration cycle. The results showed that a more effective recuperator improves internal thermal efficiency by reducing solar heat demand but reduces the system's ability to provide useful heating and cooling. This highlights a key trade-off: in applications prioritizing trigeneration (especially heating/cooling), an overly efficient recuperator may reduce overall CCHP performance. CCHP energy and exergy efficiencies decrease with increased recuperator effectiveness due to less waste heat available for heating and cooling subsystems. The drop in CCHP efficiency is more pronounced in exergy terms,

highlighting the quality loss of thermal outputs at higher effectiveness. Both electrical energy and exergy efficiencies remain essentially constant at 43.2% and 41.0%, respectively. This result is consistent with the previous figure, where net power output was unaffected by recuperator effectiveness. Since recuperator effectiveness doesn't influence turbine or compressor work directly, electrical generation performance remains stable. The CCHP system's energy efficiency decreases from ~93% at 0.50 effectiveness to about 78% at 0.80. This drop is due to the reduced availability of thermal energy in the turbine exhaust. As recuperator effectiveness increases, more internal heat is recovered, so less waste heat is available for heating and cooling loads, which form a major part of the energy efficiency metric in trigeneration systems. The CCHP exergy efficiency drops from approximately ~70% to ~57% as effectiveness increases. This reflects the decline in usable (quality) thermal energy, especially for heating applications where low-grade heat contributes little to system exergy. The more efficient the recuperator, the lower the exergy flow in the exhaust stream, resulting in a decreased overall second-law performance. COP of the absorption refrigeration cycle remains stable at around 0.82–0.83. This suggests that the absorption refrigeration system is not significantly affected by changes in recuperator effectiveness.

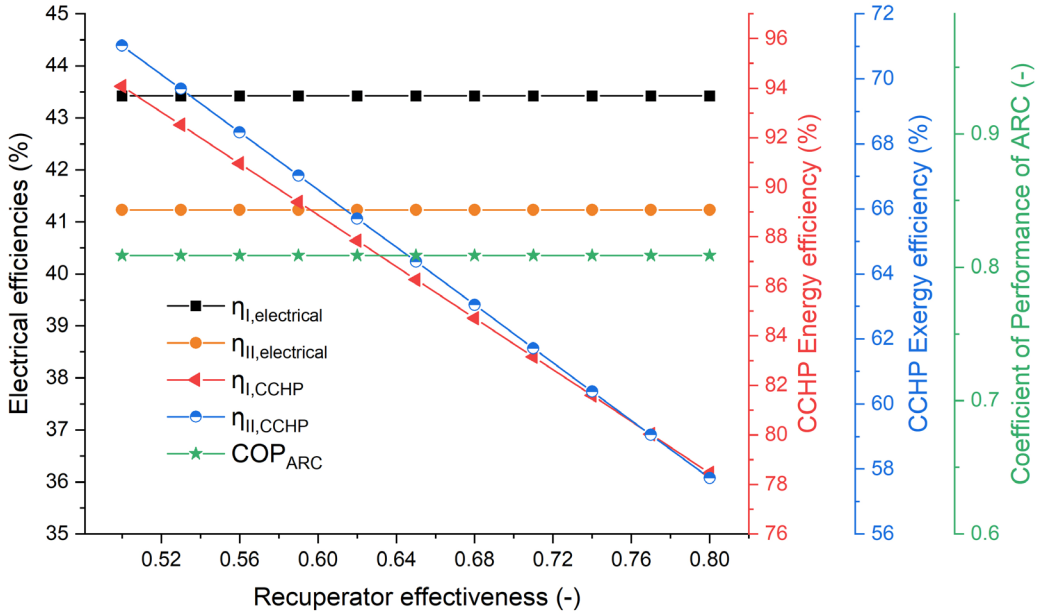

Figure 4. 8. Variation of electrical, energy, and exergy efficiencies of the CCHP system and COP of the absorption refrigeration cycle with recuperator effectiveness.

Figure 9 demonstrates how varying the heliostat area from 35,000 to 65,000 m² affects three key aspects of the solar-driven CCHP system: net electrical power output, cooling load, and heating load. The findings present the heliostat area as directly proportional to all output parameters, particularly net power and heating load. Power generation and heating benefit most from larger solar input, while cooling improves only modestly, indicating plateauing behavior due to absorption system limitations. The net power output increases significantly from ~8,900 kW at 35,000 m² to over 15,000 kW at 65,000 m². This increase is nearly linear, showing a direct relationship between the amount of solar energy collected and the mechanical/electrical power generated. As the heliostat area expands, more sunlight is focused onto the solar receiver, increasing the thermal input and thus the energy available for the Brayton cycle. The cooling load increases from ~6,720 kW to ~6,900 kW, showing a modest gain of about 180 kW. This occurs because greater thermal input leads to higher exhaust temperatures from the turbine, which powers the generator of the absorption chiller more effectively. However, the increase is less steep than net power, reflecting the limited capacity of the cooling system to utilize additional thermal energy. The heating load increases from ~8,900 kW to over 15,500 kW, following a trend nearly

identical to the net power output. This indicates that residual heat after power generation is effectively recovered and redirected for heating applications. Heating output benefits directly from higher thermal energy in the exhaust stream.

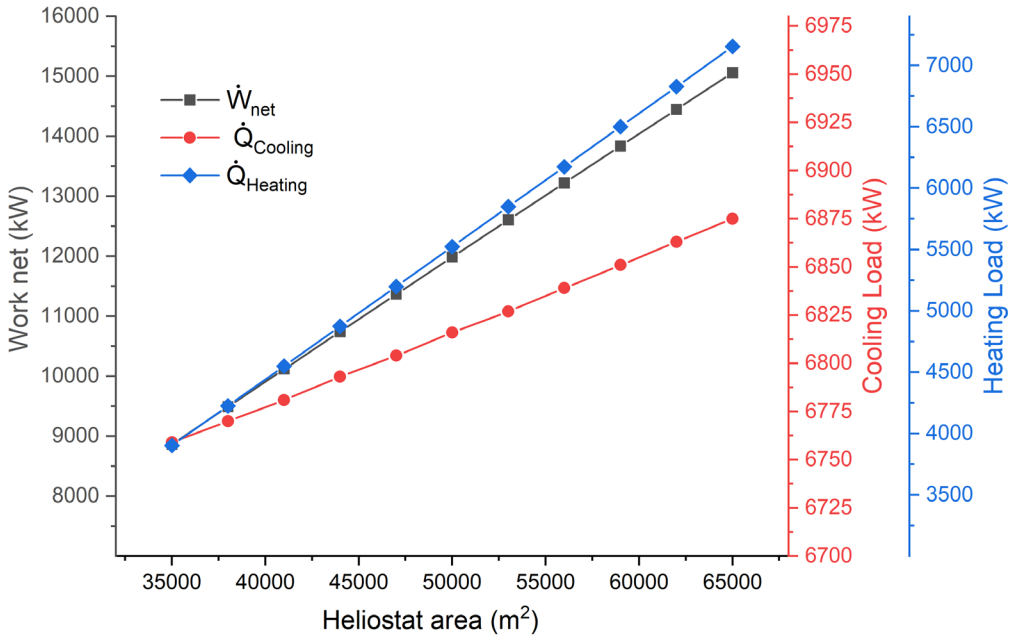

Figure 4. 9. Effect of heliostat area on net power output, cooling, and heating loads in a solar-driven CCHP system.

Figure 8 presents the effect of the increases in heliostat Area on the CCPH's electrical, energy, and exergy efficiencies and COP. The curves show that while increasing the heliostat field area does improve absolute output (power, heating, cooling), it also leads to a decline in system efficiency due to increased thermal losses and underutilization of surplus heat. Thus, optimal heliostat area sizing is critical for balancing maximum energy output and the highest system efficiency. Also, the CCHP energy efficiency decreases from about ~96% to ~77%, showing a significant decline, and CCHP exergy efficiency declines from ~66% to ~60%. These decreases result from diminishing returns in utilizing additional solar energy: The heating and cooling subsystems cannot fully absorb or utilize the surplus thermal energy. The overall system becomes less efficient in converting input energy to high-quality, useful outputs. Additionally, irreversibilities and losses grow as system size scales up, further lowering exergy efficiency. The COP_{ARC} remains nearly constant at ~0.83, regardless of the heliostat

area. This confirms that the performance of the absorption cooling system is not sensitive to the scale of solar input as long as it receives sufficient heat to operate.

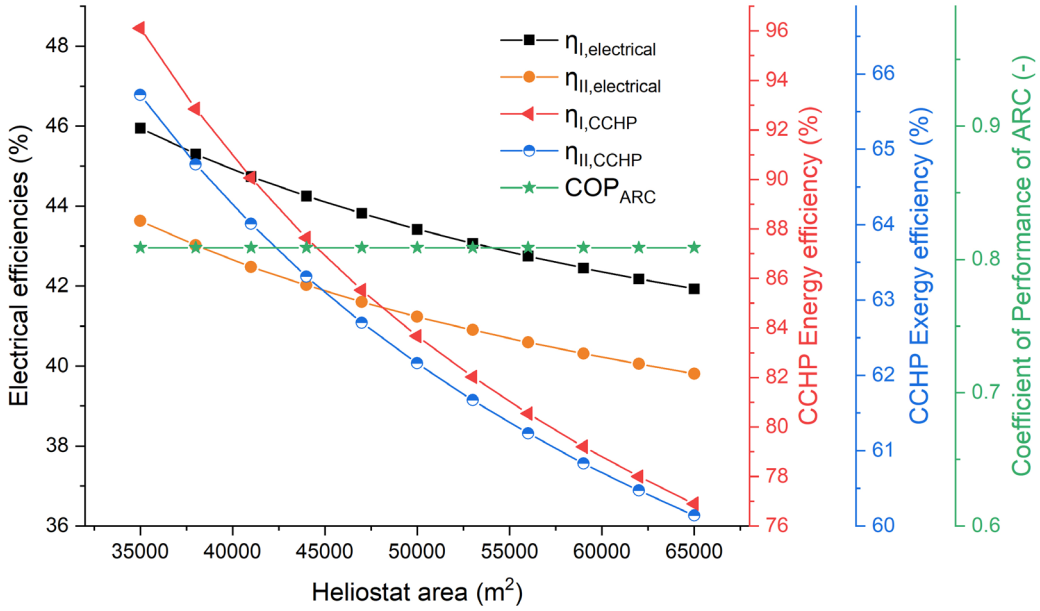

Figure 4. 10. Variation of electrical, energy, and exergy efficiencies of the CCHP system and COP of the absorption refrigeration cycle with heliostat area.

Figure 11 presents the analysis of the influence of evaporator temperature on net power, cooling, and heating loads as the evaporator temperature (T_{19}) increases from 0°C to 10°C. The findings reveal that the power and heating outputs are unaffected by changes in evaporator temperature, confirming their independence from the absorption refrigeration cycle. Cooling output increases linearly with evaporator temperature due to improved thermodynamic conditions for the absorption process. The net power output remains constant at approximately 12,000 kW across all evaporator temperatures. This is expected because the Brayton cycle generates power and is thermally independent of the absorption refrigeration cycle (where T_{19} applies). The evaporator temperature change does not affect the solar receiver, turbine, or compressor operations, hence the flat trend. The cooling load increases from ~9,200 kW at 0°C to ~9,800 kW at 10°C. This occurs because the evaporator temperature directly affects the chiller performance. As the evaporator temperature increases, less thermal energy is required for the absorption cycle to operate, improving its efficiency. This results in higher cooling capacity for the same generator heat input. The heating

load remains stable at approximately 11,000 kW. Like power output, this behavior is expected because the heating subsystem is supplied by exhaust heat and is independent of the evaporator-side changes in the absorption cycle.

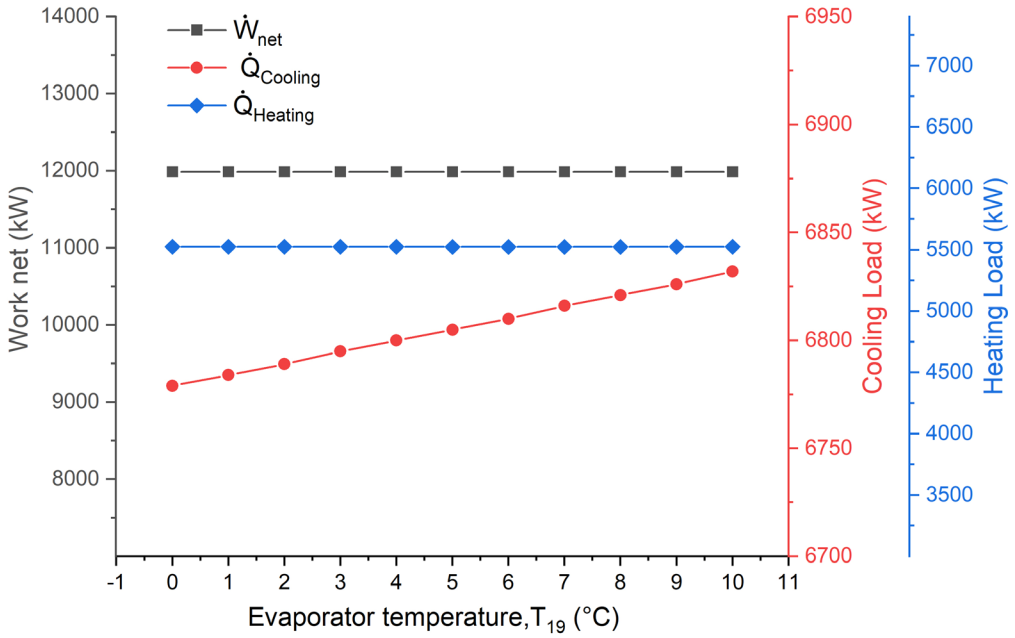

Figure 4. 11. Effect of evaporator temperature on net power output, cooling, and heating loads in a solar-driven CCHP system.

Figure 12 shows how changing the evaporator temperature from 0°C to 10°C affects CCHP system efficiencies and COP. The results show that raising the evaporator temperature offers a modest improvement in cooling efficiency (COP) and energy efficiency without negatively affecting power generation. However, from an exergy standpoint, it slightly degrades system quality due to lower temperature differentials. Electrical performance remains stable since the evaporator operates independently of the power cycle. CCHP energy efficiency slightly increases, driven by greater cooling energy recovery. Exergy efficiency drops slightly due to the reduced thermodynamic quality of the cooling effect. COP_ARC steadily improves, suggesting enhanced performance of the absorption system with higher evaporator temperatures. Both first-law and second-law electrical efficiencies remain nearly constant across the temperature range: $\eta_{I,electrical} \approx 43.4\%$, and $\eta_{II,electrical} \approx 41.8\%$. This behavior is expected because evaporator temperature affects only the absorption cooling subsystem and does not influence the solar collector, turbine, or compressor that governs electrical

output. The energy efficiency of the CCHP system increases slightly, from about 84.1% to 84.4%. This subtle improvement results from the enhanced cooling load at higher evaporator temperatures (as seen in Figure 9), which contributes more to the total useful energy output. The exergy efficiency drops from ~40.1% to ~39.0% as $T19$ rises. This is due to the decreasing exergy content of the cooling output. As the evaporator temperature increases, the temperature difference between the evaporator and the environment decreases, reducing the exergy value of the cooling effect. Even though the system provides more cooling in terms of energy, its quality (usefulness) decreases from a second-law standpoint. The coefficient of performance (COP_{ARC}) improves from ~0.81 to ~0.835. This trend reflects the improved thermodynamic performance of the ARC at higher evaporator temperatures. With a smaller lift between the evaporator and condenser/generator temperatures, the system becomes more efficient in converting heat into cooling.

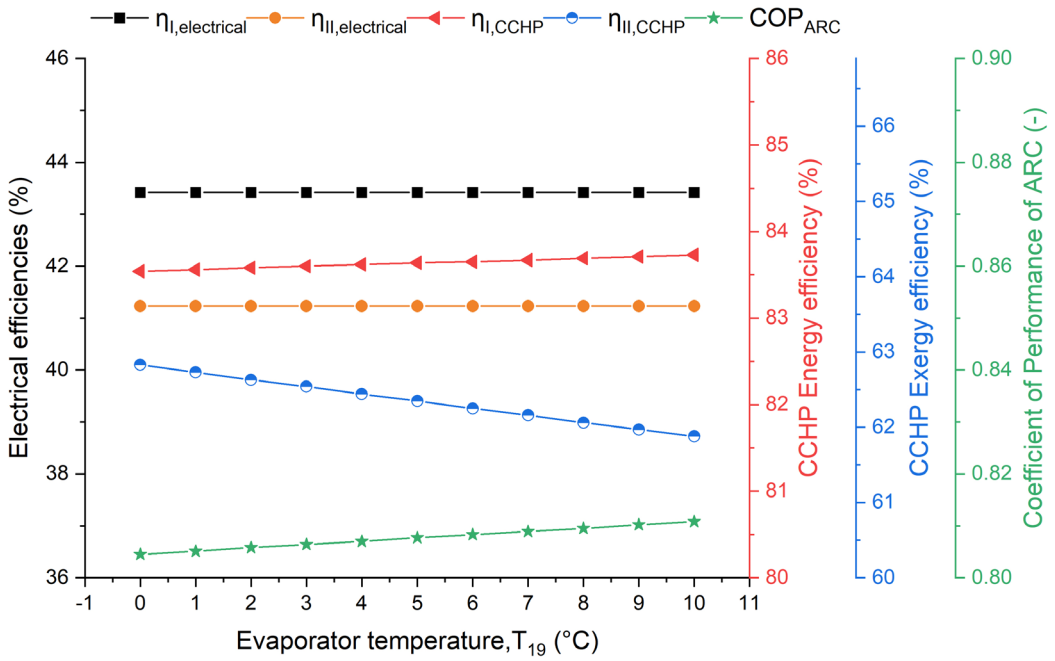

Figure 4. 12. Variation of electrical, energy, and exergy efficiencies of the CCHP system and COP of the absorption refrigeration cycle with evaporator temperature, T_{19}.

Figure 13 presents the analysis of the impact of varying the generator temperature from 80°C to 100°C on CCHP outputs. The findings present that the power and heating output remain unaffected by changes in generator temperature, while the cooling load

drops significantly as the generator temperature increases, indicating that the absorption refrigeration cycle is highly sensitive to this parameter. The generator temperature must be optimized to ensure maximum cooling performance in solar-driven CCHP systems. Operating the generator above 85–90°C can reduce cooling capacity significantly, which may affect system performance in cooling-dominated applications. The net power output remains constant at around 11,950–12,000 kW across the full range of $T14$. This is because the generator temperature in the absorption refrigeration cycle does not affect Brayton cycle, which is responsible for producing electrical power. Thus, the power generation subsystem is thermally decoupled from changes in generator operating conditions. The cooling load decreases significantly, from approximately 13,200 kW at 80°C to 8,000 kW at 100°C. This is due to the inverse relationship between generator temperature and the absorption chiller's cooling capacity. At lower generator temperatures, the absorption cycle performs better because the working fluid (LiBr-H2O solution) maintains a more favorable balance between absorption and desorption. At higher temperatures, performance declines due to increased irreversibilities and poorer thermodynamic matching within the cycle. The heating load remains constant at approximately 11,000 kW. This is expected, as the heating subsystem is based on exhaust heat recovery from the turbine and is not influenced by the generator temperature of the absorption chiller.

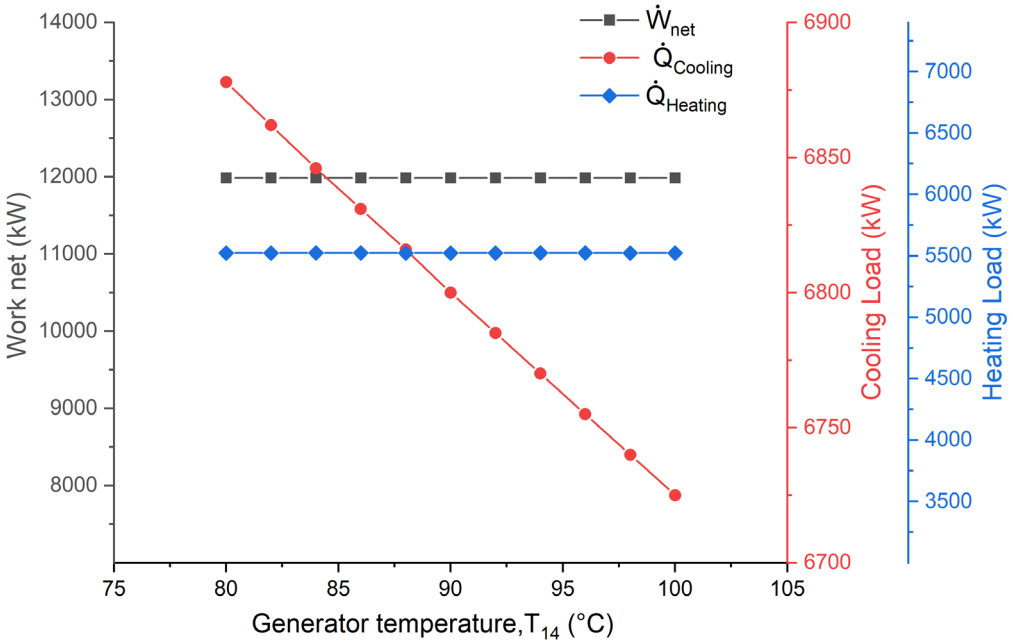

Figure 4. 13. Effect of generator temperature (T_{14}) on net power output, cooling, and heating loads in a solar-driven CCHP system.

Figure 14 plots the variation of the following parameters with generator temperature ranging from 80°C to 100°C: First-law electrical efficiency ($\eta_{I,electrical}$), Second-law electrical efficiency ($\eta_{II,electrical}$), CCHP energy efficiency ($\eta_{I,CCHP}$), CCHP eXergy efficiency ($\eta_{II,CCHP}$), and Coefficient of Performance of ARC. The results show that the generator temperature must be carefully controlled to maximize cooling efficiency and maintain overall system performance. The electrical performance is unaffected by generator temperature, confirming the independence of the power subsystem. CCHP energy and exergy efficiencies decline, primarily due to reduced cooling performance of the absorption refrigeration cycle. COP_{ARC} also decreases, reflecting poorer thermal efficiency at higher generator temperatures due to increased system irreversibility. Both first- and second-law electrical efficiencies remain stable across the generator temperature range: $\eta_{I,electrical} \approx 43.2\%$ and $\eta_{II,electrical} \approx 41.8\%$. This trend indicates that generator temperature changes do not influence the power cycle (Brayton cycle), which is thermodynamically isolated from the absorption generator. The energy efficiency of the entire CCHP system decreases steadily from ~43.0% to ~42.0%. This is due to the decline in cooling output as generator temperature increases (as confirmed in Figure 11). Since $\eta_{I,CCHP}$ and $\eta_{II,CCHP}$ includes the sum of electrical, heating, and cooling outputs, reducing any component (here, cooling) leads to a lower overall

efficiency. Exergy efficiency falls slightly, from ~40.0% to ~39.0% as $T14$ increases. The reduction is smaller than energy efficiency because exergy focuses on the quality of energy. While cooling quantity drops, its exergy value also drops due to smaller thermal gradients, leading to a modest overall effect. COP decreases from ~0.815 to ~0.785 over the temperature range. This trend is consistent with thermodynamic principles. At higher generator temperatures, the absorption process becomes less efficient due to increased irreversibilities. The energy required for desorption rises disproportionately, reducing the cooling effect per unit of heat input.

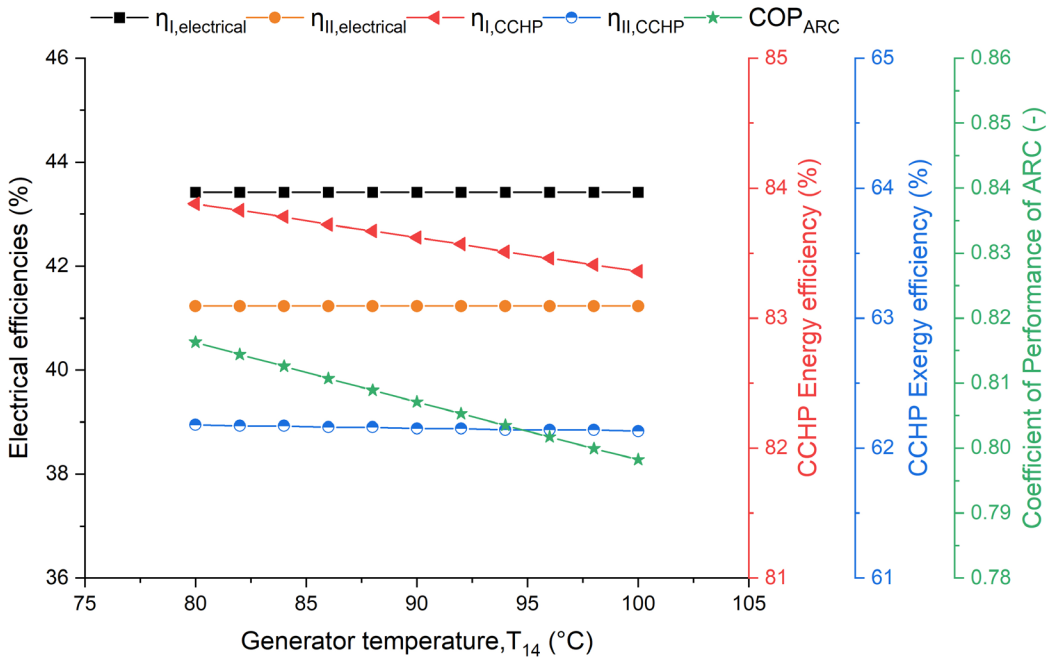

Figure 4. 14. Variation of electrical, energy, and exergy efficiencies of the CCHP system and COP of the absorption refrigeration cycle with generator temperature(T_{14}).

Figure 13 presents the analysis of the impact of generator exit temperature ($T17$) on system performance. The generator exit temperature is a key design variable in balancing cooling versus heating outputs in CCHP systems. The findings showed that the electrical power output remains unaffected, affirming the thermal separation between the generator and Brayton cycle, while the cooling load decreases as the generator exit temperature rises, indicating lower thermal utilization in the absorption generator. The heating load increases, confirming that more residual thermal energy is available in the fluid after leaving the generator. This reflects a clear trade-off between

cooling and heating performance based on how much thermal energy is extracted in the generator. The net power output remains nearly constant at around 11,950–12,000 kW. This indicates that changes in the generator exit temperature (after heat is extracted for the absorption chiller) do not affect the solar-powered Brayton cycle, which dominates electrical power production. The cooling load decreases significantly, from about 13,300 kW at 200°C to ~4,500 kW at 300°C. This trend shows that as the generator exit temperature increases, the effectiveness of the absorption cooling cycle diminishes. A higher exit temperature implies less heat is being absorbed by the refrigerant in the generator (LiBr-H_2O solution), which directly reduces the driving thermal energy for the cooling process. The heating load increases sharply from ~8,300 kW at 200°C to ~8,2000 kW (8 MW) at 300°C. This is because more unused thermal energy remains in the working fluid, which can now be recovered through heat exchangers for heating purposes. Essentially, less energy is consumed in the generator, and more is left in the exhaust, which can be redirected to meet heating demand.

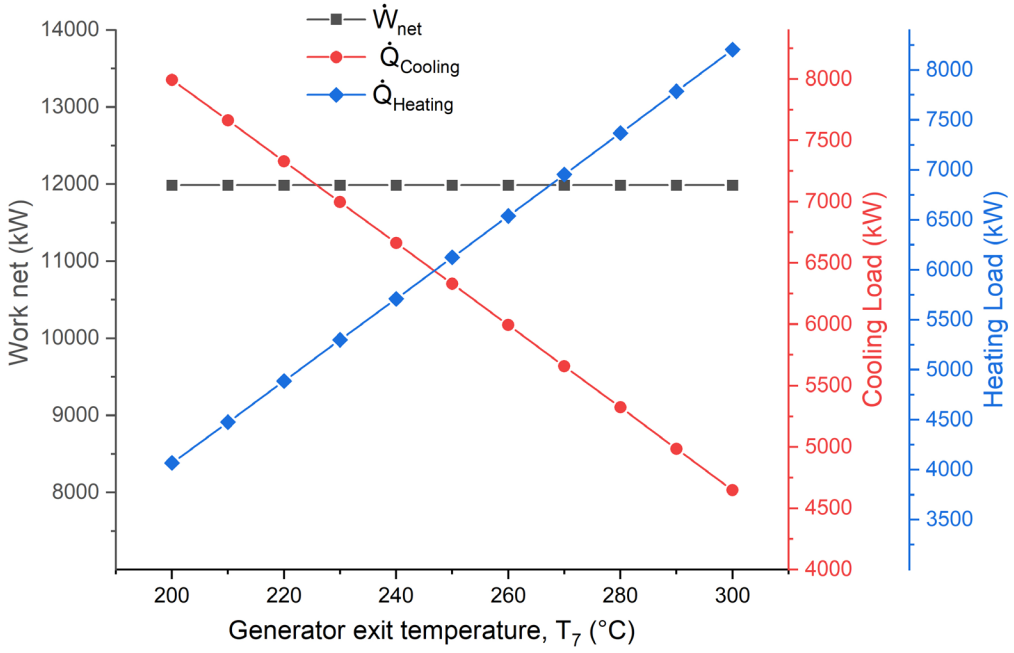

Figure 4. 15. Effect of generator exit temperature (T_{14}) on net power output, cooling, and heating loads in a solar-driven CCHP system.

Figure 14 presents the variation of the following parameters with generator exit temperature ranging from 200°C to 300°C: First-law electrical efficiency ($\eta_{I,electrical}$),

Second-law electrical efficiency ($\eta_{II,electrical}$), CCHP energy efficiency ($\eta_{I,CCHP}$), CCHP exergy efficiency ($\eta_{II,CCHP}$), and coefficient of performance of ARC. These findings reveal that higher generator exit temperatures benefit total system efficiency by improving heat recovery, even though cooling output declines (as shown in earlier figures). Both first- and second-law electrical efficiencies remain stable across the generator temperature range: $\eta_{I,electrical} \approx 43.2\%$ and $\eta_{II,electrical} \approx 41.8\%$. This confirms that generator exit temperature does not influence the power cycle, as the solar-powered Brayton cycle is independent of the absorption generator outlet. The CCHP energy efficiency increases from ~38% to ~44% as T7 increases. This is a result of increased heating load at higher generator exit temperatures (as seen in Figure 15), meaning more thermal energy is recovered and utilized. Although cooling load drops (per previous analysis), the increase in recoverable heat energy outweighs the cooling loss, leading to an improvement in total energy utilization. Also, the CCHP exergy efficiency increases from ~37% to ~44% as T7 rises. This indicates an improvement in the quality and quantity of useful energy (power + heat) extracted from the system. As heating loads grow, the availability of high-grade thermal energy for useful work increases, boosting the second-law performance of the CCHP system. COP remains almost flat at around 0.81, indicating that the performance of the absorption refrigeration cycle is not significantly affected by the generator exit temperature. This is because COP primarily depends on generator inlet temperature, evaporator temperature, and condenser conditions not the outlet.

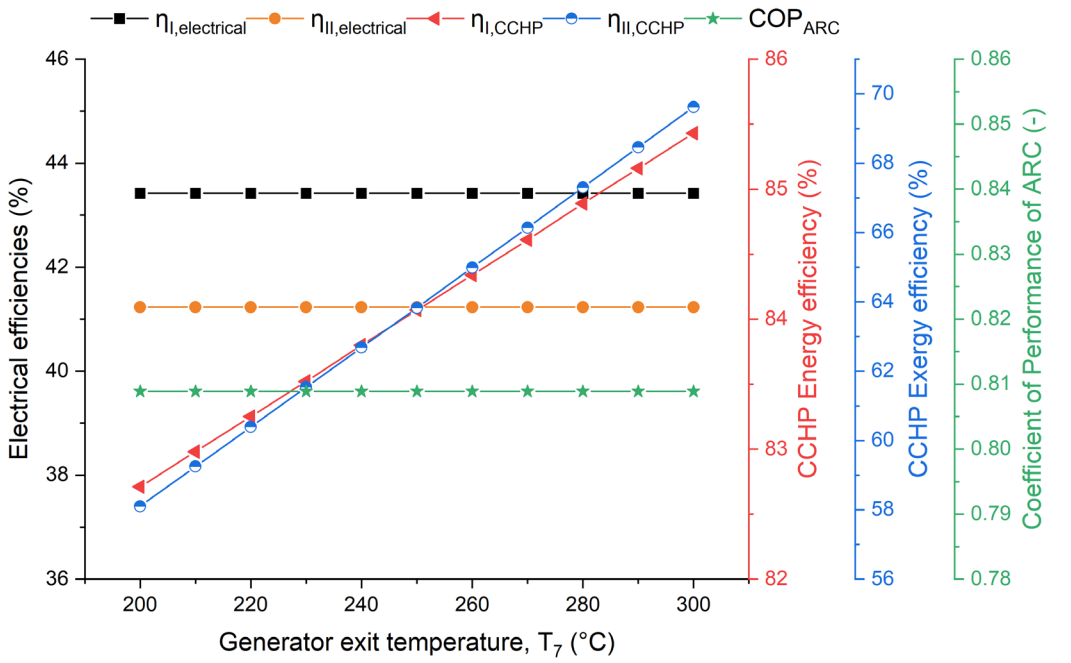

Figure 4. 16. Variation of electrical, energy, and exergy efficiencies of the CCHP system and COP of the absorption refrigeration cycle with generator exit temperature(T_7).

4.5 COMPARATIVE MONTHLY ANALYSIS OF SOLAR-DRIVEN CCHP SYSTEM IN TRIPOLI

Table 4.4 presents a comparative analysis of monthly performance indicators of a solar-driven CCHP system in Tripoli. The analysis includes Direct Normal Irradiance (DNI), net power output, heating load, and cooling load. These parameters reflect the seasonal behavior of the system and the effectiveness of solar energy utilization throughout the year. The solar-driven CCHP system in Tripoli demonstrates strong seasonal performance trends. It efficiently harnesses solar energy for both electrical and thermal applications, especially in the summer months. The relatively stable cooling load year-round reflects operational reliability. The DNI increases from January, peaking in July (778 kWh/m²·day), then declines toward December. This pattern matches the net power output, which also reaches a maximum in July (11703 kW). Heating load shows a gradual increase from January (3185 kW) to July (5374 kW), indicating a higher thermal demand in warmer months, possibly for industrial heating or absorption cooling. Cooling load remains relatively stable throughout the

year, with minor variations, peaking in July (6810 kW). This stability suggests consistent cooling demand or controlled system design.

Table 4. 4. Comparative analysis of monthly performance indicators of a solar-driven CCHP system in Tripoli

Month	DNI (kWh/m²·day)	Work Net (kW)	Heating Load (kW)	Cooling Load (kW)
Jan	453	7450	3185	6734
Feb	499	8059	3493	6745
Mar	573	9033	3991	6762
Apr	634	9832	4401	6776
May	699	10679	4840	6791
Jun	755	11405	5218	6805
Jul	778	11703	5374	6810
Aug	714	10874	4941	6795
Sep	611	9531	4246	6771
Oct	531	8481	3708	6752
Nov	478	7781	3353	6740
Dec	436	7225	3071	6730

Figure 4.17 provides a monthly analysis of direct normal solar radiation (DNI) in Tripoli, measured in kWh/m² day. DNI data for Tripoli show a clear seasonal pattern consistent with the typical solar distribution in Mediterranean climates; summers are rich in solar radiation, while winters are less productive. The data shows that the amount of solar radiation gradually increases from January to July, reaching its peak in July (778 kWh/m² day). It then begins to gradually decrease until it reaches its lowest value in December (436 kWh/m² day). The three highest months in terms of radiation are July (778 kWh/m² day), June (755 kWh/m² day), and August (714 kWh/m² day). The three lowest months in terms of radiation are December (436 kWh/m² day), January (453 kWh/m² day), and November (478 kWh/m² day). The period from April to August represents the solar peak, which is ideal for solar power generation using concentrating solar power systems (such as solar towers or parabolic mirrors). January and December represent the minimum in terms of solar production, which may require the use of auxiliary energy sources during those months. This

supports the feasibility of using concentrated solar power (CSP) systems in Libya, especially during the summer months.

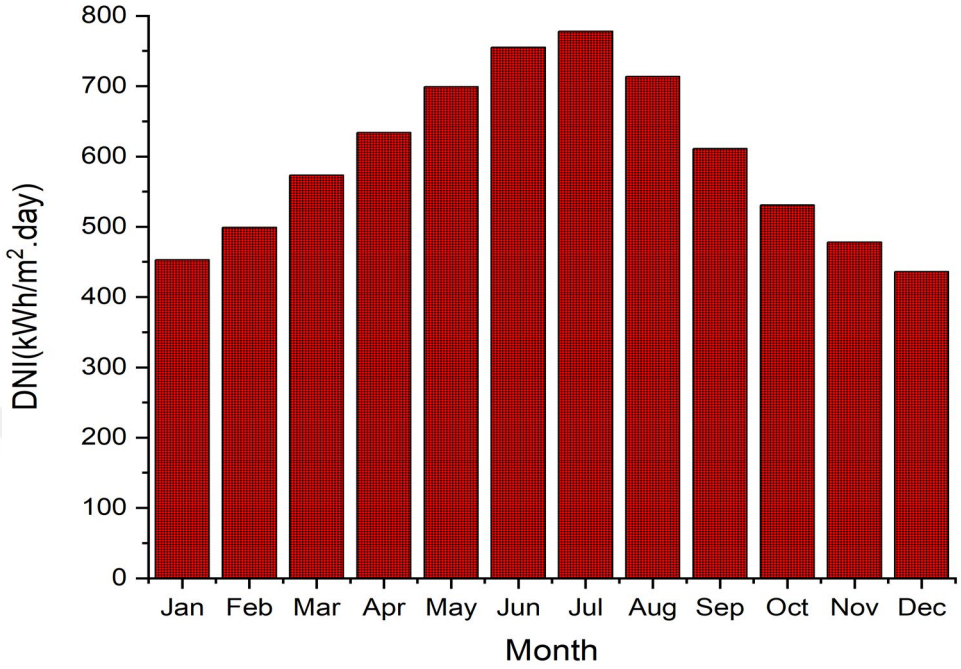

Figure 4. 17. Monthly Average Direct Normal Irradiance (DNI) Profile for Tripoli.

Figure 4. 18 illustrates the monthly variation in net power output from a solar-powered CCHP system in Tripoli. The solar-powered CCHP system in Tripoli demonstrates high seasonal performance directly linked to solar radiation. The summer months represent ideal opportunities for high energy production, indicating that these systems are highly effective in Tripoli's climate, especially during the summer. There is a gradual increase in net power output from January until it reaches its peak in July (11,703 kW). Then, the capacity begins to gradually decline from August until December, recording its lowest value in December (7,225 kW). There is a strong agreement between the work net power output values and the DNI (direct solar irradiance) values in the previous analysis, demonstrating the system's efficiency in converting solar energy into electrical energy. Peak months are June, July, and August, the same as the peak solar months. The lowest output is in December and January, due to low solar irradiance.

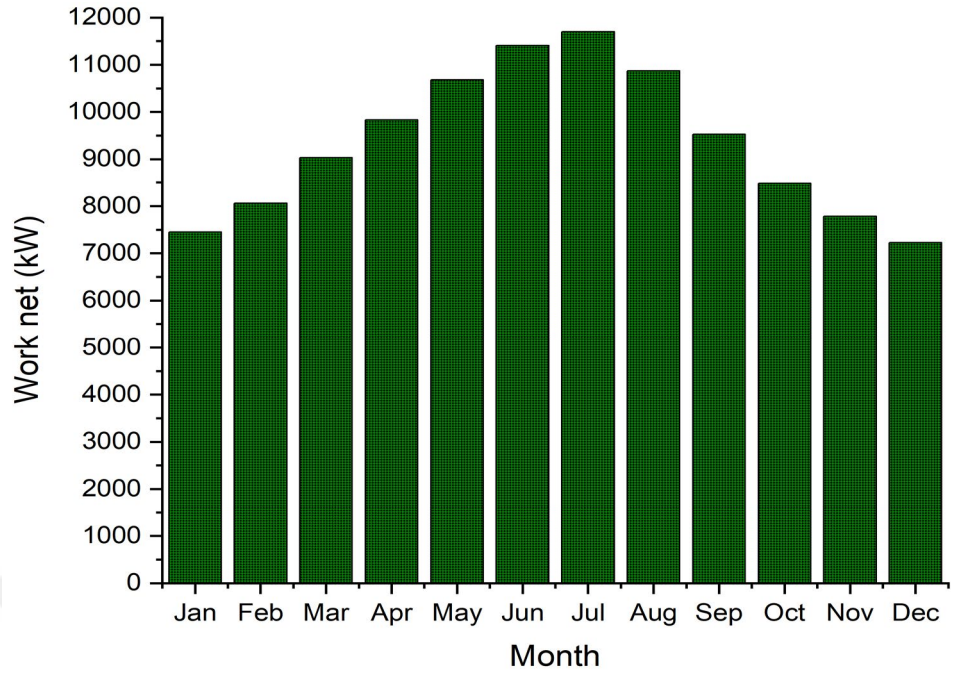

Figure 4. 18. Monthly Variation of Net Power Output from the solar-driven CCHP in Tripoli.

Figure 4.19 shows the monthly variation in the heating load met by a solar-powered CCHP system in Tripoli, in kW. The findings present that this system is effective in Tripoli's climate, provided that demand management is effective during the winter. The heat load curve exhibits a bell-shaped pattern, where it starts low in January (3185 kW), it gradually increases to a peak in July (5374 kW), and it then decreases again until it reaches its lowest value in December (3071 kW). July records the highest heat load because it's the hottest month in terms of solar radiation. The lowest load values are in January and December, indicating that the system is not only used for winter residential heating, but also for other heating needs throughout the year. There is a direct relationship between heat load and net power output (work net), indicating that the thermal system responds directly to available solar radiation. Heat load increases in the same pattern as solar radiation and net power output, demonstrating the system's efficiency in utilizing solar energy to meet thermal demand. The CCHP system in Tripoli meets consistent heat demand year-round, with a pronounced peak in the summer.

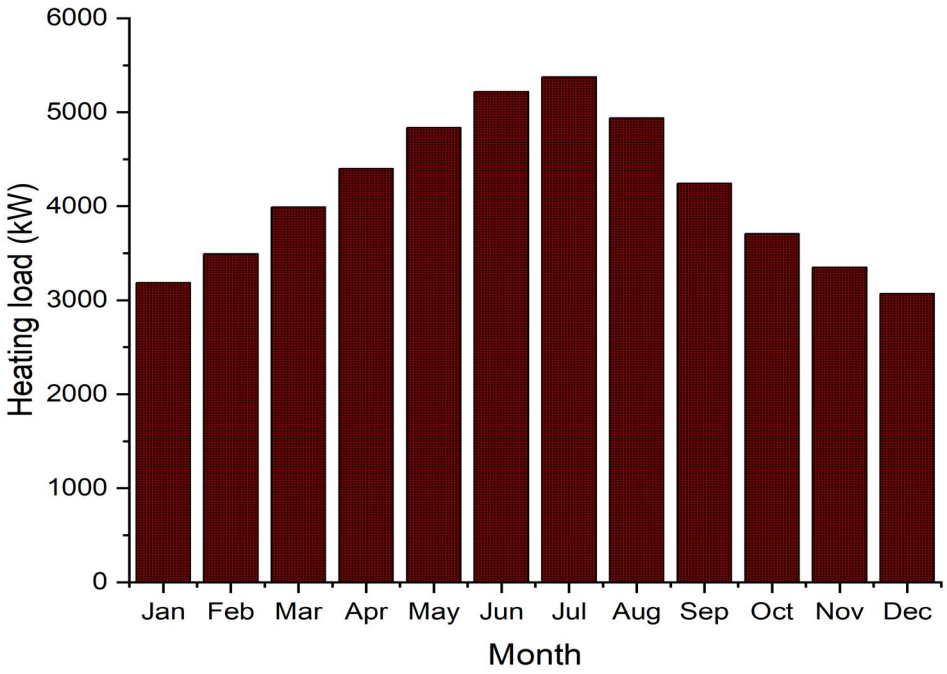

Figure 4. 19. Monthly Variation of Heating Load Supplied by the solar-driven CCHP system in Tripoli.

Figure 4.20 demonstrates the monthly variation in cooling load for a solar CCHP system in Tripoli. The results show that the CCHP system in Tripoli operates efficiently in stabilizing the cooling load throughout the year, despite changes in solar radiation and heat load. There is a slight increase in cooling load from January (6734 kW) to a peak in July (6810 kW). The load then begins a slight decline until it reaches December (6730 kW). The monthly variation is very small (less than 100 kW difference between adjacent months), indicating a significant stability in cooling demand throughout the year. A slight peak in July corresponds to the highest DNI and solar radiation values. While the heat load and electrical production exhibit significant seasonal fluctuations, the cooling load is relatively constant.

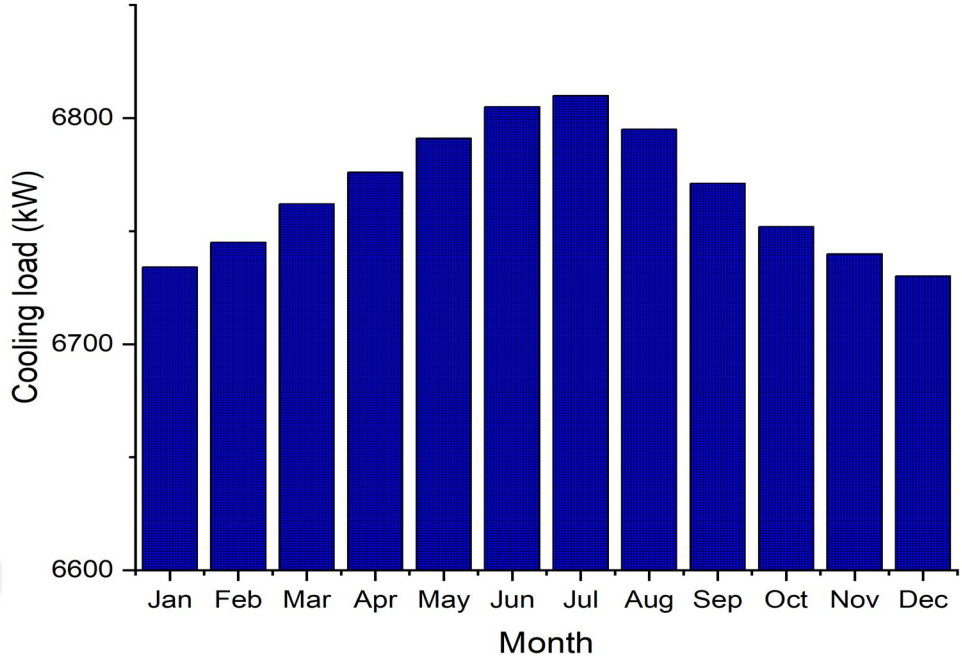

Figure 4. 20. Monthly Variation of Cooling Load Supplied by the solar-driven CCHP system in Tripoli.

CHAPTER 5

CONCLUSION AND FUTURE WORK

This study presented the modeling, simulation, and performance evaluation of a novel solar-powered Combined Cooling, Heating, and Power (CCHP) system incorporating a regenerative Brayton cycle and an absorption refrigeration system (ARS), specifically adapted to the environmental and energy context of Libya. The motivation for this research arises from the critical need to develop sustainable and efficient energy systems that leverage Libya's abundant solar resources, reduce dependence on fossil fuels, and address the increasing demands for electricity, heating, and cooling. A comprehensive thermodynamic model was developed, focusing on both energy and exergy analyses to provide a thorough assessment of the system's performance. The originality of the present work lies in the exclusive reliance on solar thermal energy to drive a regenerative Brayton cycle integrated with an ARS, a configuration not previously explored in the literature for Libya. The ARS subsystem was validated using benchmark data from previous studies, ensuring the reliability of the model outputs. Due to the absence of comparable solar regenerative Brayton cycle models in the literature, the current system was modeled independently, further underscoring the novelty of the research. Detailed exergy destruction analysis and a parametric study examining the effect of pressure ratio variations were conducted to identify major sources of inefficiencies and potential pathways for system optimization.

The principal findings of this study are summarized as follows:

- The heating and cooling loads were determined to be 5,523 kW and 6,816 kW, respectively, confirming the system's capability to meet multiple energy demands.

- The proposed system achieved a net electrical output of 11,987 kW, demonstrating a high capacity for power generation.
- The overall exergy efficiency was calculated at 45.59%, reflecting a moderate level of thermodynamic performance considering system irreversibilities**.**
- The absorption refrigeration subsystem achieved a coefficient of performance (COP) of approximately 0.81, consistent with expected values for single-effect LiBr-water systems.
- The system exhibited an overall CCHP energy efficiency of 83.67%, indicating efficient utilization of the solar energy input.
- The exergy destruction analysis identified the **steam reformer** as the primary source of inefficiencies, responsible for approximately **45.33%** of the total exergy destruction.
- High exergy efficiencies were observed for the gas turbine and solar receiver, exceeding 88%, underscoring their effective energy conversion capabilities.
- The parametric analysis revealed that increasing the pressure ratio positively influences the net power output, while slightly reducing the heating and cooling capacities.

In light of these results, several recommendations are proposed for future work. Future research could explore the integration of thermal and electrical energy storage systems to enhance the reliability and flexibility of solar combined heat and power (CCHP) system configurations, especially during periods of low solar radiation. A comprehensive techno-economic feasibility study is also recommended to assess the feasibility of deploying the proposed system on a large scale in Libya.

REFERENCES

1. Creutzig, F., Simoes, S. G., Leipold, S., Berrill, P., Azevedo, I., Edelenbosch, O., Fishman, T., Haberl, H., Hertwich, E., and Krey, V., "Demand-side strategies key for mitigating material impacts of energy transitions", *Nature Climate Change*, 14 (6): 561–572 (2024).

2. Chen, N. and Usman, M., "Energy Use, Energy Depletion, and Environmental Degradation: Exploitation of Natural Resources", (2025).

3. Lane, T. P., King, A. D., Perkins-Kirkpatrick, S. E., Pitman, A. J., Alexander, L. V, Arblaster, J. M., Bindoff, N. L., Bishop, C. H., Black, M. T., and Bradstock, R. A., "Attribution of extreme events to climate change in the Australian region–A review", *Weather And Climate Extremes*, 42: 100622 (2023).

4. Clarke, B., Otto, F., Stuart-Smith, R., and Harrington, L., "Extreme weather impacts of climate change: an attribution perspective", *Environmental Research: Climate*, 1 (1): 012001 (2022).

5. Wu, D. W. and Wang, R. Z., "Combined cooling, heating and power: A review", *Progress In Energy And Combustion Science*, 32 (5–6): 459–495 (2006).

6. Wang, J., Han, Z., and Guan, Z., "Hybrid solar-assisted combined cooling, heating, and power systems: A review", *Renewable And Sustainable Energy Reviews*, 133: 110256 (2020).

7. Dincer, I., "Renewable energy and sustainable development: a crucial review", *Renewable And Sustainable Energy Reviews*, 4 (2): 157–175 (2000).

8. Hassan, Q., Al-Hitmi, M., Tabar, V. S., Sameen, A. Z., Salman, H. M., and Jaszczur, M., "RETRACTED: Middle East energy consumption and potential renewable sources: An overview", *Cleaner Engineering And Technology*, 12: 100599 (2023).

9. El Bassam, N., "Technologies and options of solar energy applications in the Middle East", *Water, Energy & Food Sustainability In The Middle East: The Sustainability Triangle*, 193–221 (2017).

10. Fumo, N., Chamra, L. M., and Bortone, V., "Potential of solar thermal energy for CCHP systems", (2009).

11. Eshtaiwi, S., Aburwais, M., Elsanusi, O., Elayeb, M., and Shetwan, M., "The Impact of Residential Optimally Designed Rooftop PV System on Libya Power Shortage Case", *Journal Of Energy: Energija*, 71 (3.): 3–9 (2022).

12. Khalil, A., Rajab, Z., Amhammed, M., and Asheibi, A., "The benefits of the transition from fossil fuel to solar energy in Libya: A street lighting system case study", *Applied Solar Energy*, 53: 138–151 (2017).

13. Baka, M. M. A. and Eryildiz, D. I., "The Possibility of Developing Existing Residential Buldings by Installing Photovoltaic Modules Case Study: Libya–Zuwarah", *European Journal Of Engineering And Technology Research*, 6 (4): 45–56 (2021).

14. Khalil, A., Rajab, Z., Amhammed, M., and Asheibi, A., "The benefits of the transition from fossil fuel to solar energy in Libya: A street lighting system case study", *Applied Solar Energy*, 53: 138–151 (2017).

15. Saxena, V., Manna, S., Rajput, S. K., Diwania, S., and Gupta, V., "Sustainable energy solutions: integrating hybrid CCHP systems with renewable technologies for efficient urban development", *Journal Of The Brazilian Society Of Mechanical Sciences And Engineering*, 46 (11): 668 (2024).

16. Calise, F., Vicidomini, M., Cappiello, F. L., and D'Accadia, M. D., "Combined cooling, heat, and power systems", *Polygeneration Systems*, 289–322 (2022).

17. Akroot, A. and Refaei, M., "Thermodynamic and Exergoeconomic Assessment of a Solar-Assisted Combined Cooling, Heating, and Power System in Antalya, Turkey", *Gazi Üniversitesi Fen Bilimleri Dergisi Part C: Tasarım Ve Teknoloji*, 1 (2025).

18. Qu, S., Ma, F., Ge, X., and Wang, D., "The Contribution of Thermal Energy Storage to the Energy Efficiency of Combined Cooling, Heating and Power Systems", *Procedia Engineering*, 146: 83–88 (2016).

19. Jiang, R. and Yang, X., "Performance analysis and application of a novel combined cooling, heating and power system integrated with multi-energy storage system", *Journal Of Energy Storage*, 86: 111276 (2024).

20. Fumo, N. and Chamra, L. M., "Analysis of combined cooling, heating, and power systems based on source primary energy consumption", *Applied Energy*, 87 (6): 2023–2030 (2010).

21. Kong, X. Q., Wang, R. Z., Li, Y., and Huang, X. H., "Optimal operation of a micro-combined cooling, heating and power system driven by a gas engine", *Energy Conversion And Management*, 50 (3): 530–538 (2009).

22. Fumo, N. and Chamra, L. M., "Analysis of combined cooling, heating, and power systems based on source primary energy consumption", *Applied Energy*, 87 (6): 2023–2030 (2010).

23. Liu, Z., Gao, W., Qian, F., Zhang, L., and Kuroki, S., "Potential analysis and optimization of combined cooling, heating, and power (cchp) systems for eco-campus design based on comprehensive performance assessment", *Frontiers In Energy Research*, 9: 781634 (2021).

24. Salimi, M., Hosseinpour, M., Mansouri, S., and N. Borhani, T., "Environmental aspects of the combined cooling, heating, and power (CCHP) systems: a review", *Processes*, 10 (4): 711 (2022).

25. Fumo, N., Mago, P. J., and Chamra, L. M., "Hybrid-cooling, combined cooling, heating, and power systems", *Proceedings Of The Institution Of Mechanical Engineers, Part A: Journal Of Power And Energy*, 223 (5): 487–495 (2009).

26. Ukaegbu, U., Tartibu, L., and Lim, C. W., "Optimization of Solar-Assisted CCHP Systems: Enhancing Efficiency and Reducing Emissions Through Harris Hawks-Based Mathematical Modeling", *Sustainability*, 16 (23): 10694 (2024).

27. Wang, J., Han, Z., and Guan, Z., "Hybrid solar-assisted combined cooling, heating, and power systems: A review", *Renewable And Sustainable Energy Reviews*, 133: 110256 (2020).

28. Akroot, A. and Al Shammre, A. S., "Techno-Economic and Environmental Impact Analysis of a 50 MW Solar-Powered Rankine Cycle System", *Processes*, 12 (6): 1059 (2024).

29. Kassem, Y., Camur, H., and Abughinda, O. A. M., "Solar energy potential and feasibility study of a 10MW grid-connected solar plant in Libya", *Engineering, Technology & Applied Science Research*, 10 (4): 5358–5366 (2020).

30. Yang, G. and Zhai, X. Q., "Optimal design and performance analysis of solar hybrid CCHP system considering influence of building type and climate condition", *Energy*, 174: 647–663 (2019).

31. Greppi, M. and Fabbri, G., "Integrated apparatus for supporting and cooling a photovoltaic panel", *Invention Disclosure*, 4: 100019 (2024).

32. AlOtaibi, Z. S., Khonkar, H. I., AlAmoudi, A. O., and Alqahtani, S. H., "Current status and future perspectives for localizing the solar photovoltaic industry in the Kingdom of Saudi Arabia", *Energy Transitions*, 4: 1–9 (2020).

33. Bataineh, K., "Hybrid fuel-assisted solar-powered stirling engine for combined cooling, heating, and power systems: A review", *Energy*, 300: 131506 (2024).

34. Wu, H., Liu, Q., Xie, G., Guo, S., Zheng, J., and Su, B., "Performance investigation of a novel hybrid combined cooling, heating and power system with solar thermochemistry in different climate zones", *Energy*, 190: 116281 (2020).

35. Chen, L., Shen, J., Ge, Y., Wu, Z., Wang, W., Zhu, F., and Feng, H., "Power and efficiency optimization of open Maisotsenko-Brayton cycle and performance comparison with traditional open regenerated Brayton cycle", *Energy Conversion And Management*, 217: 113001 (2020).

36. Goodarzi, M., "Comparative energy analysis on a new regenerative Brayton cycle", *Energy Conversion And Management*, 120: 25–31 (2016).

37. Abbas, A., Luu, M., Milani, D., and McNaughton, R., "A comparative study of solar heliostat assisted supercritical CO 2 recompression Brayton cycles: Dynamic modelling and control strategies", (2017).

38. Milani, D., Luu, M. T., McNaughton, R., and Abbas, A., "A comparative study of solar heliostat assisted supercritical CO2 recompression Brayton cycles: dynamic modelling and control strategies", *The Journal Of Supercritical Fluids*, 120: 113–124 (2017).

39. Hassanlue, S., Mukhtar, A., Yasir, A. S. H. M., Eldin, S. M., Nazari, M. A., Ahmadi, M. H., and Sharifpur, M., "Sensitivity analysis and thermodynamic evaluation of a combined cooling, heating and power system utilizing exhaust gases of smelting furnace", *Heliyon*, 10 (5): (2024).

40. Elbaksawi, O., Elminshawy, N. A. S., Diab, S., Eltamaly, A. M., Mahmoud, A., and Elhadidy, H., "Innovative metaheuristic algorithm with comparative analysis of MPPT for 5.5 kW floating photovoltaic system", *Process Safety And Environmental Protection*, 185: 1072–1088 (2024).

41. Alhuyi-Nazari, M., Mukhtar, A., Yasir, A. S. H. M., Ahmadi, M. H., Kumar, R., and Luong, T. N. L., "Applications of geothermal sources for absorption chillers as efficient and clean cooling technologies for buildings: A comprehensive review", *Journal Of Building Engineering*, 82: 108340 (2024).

42. Salimi, M., Hosseinpour, M., Mansouri, S., and N. Borhani, T., "Environmental aspects of the combined cooling, heating, and power (CCHP) systems: a review", *Processes*, 10 (4): 711 (2022).

43. Camara, S., Sulin, A. B., and Coulibaly, S., "Design and performance study of a double-acting collector-assisted absorption cooling system in a hot region", *Cleaner Energy Systems*, 7: 100099 (2024).

44. Gunawan, S., Arfianto, W., and Heryadi, B., "A Comparative Review and Novel Design Possibilities on Solar-Driven Absorption LiBr-H2O Refrigeration System", (2024).

45. Ali, F. H., Al-Amir, Q. R., Hamzah, H. K., and Alahmer, A., "Unveiling the potential of solar cooling technologies for sustainable energy and environmental solutions", *Energy Conversion And Management*, 321: 119034 (2024).

46. Gomri, R., "Second law comparison of single effect and double effect vapour absorption refrigeration systems", *Energy Conversion And Management*, 50 (5): 1279–1287 (2009).

47. Eliaser, A. O., "CHALLENGES AND OPPORUNITIES TO TRANSITION INTO A KNOWLEDGE-BASED ECONOMY IN LIBYA", *KNOWLEDGE BASED SUSTAINABLE DEVELOPMENT*, 117 (2020).

48. Mohamed, O. A. and Masood, S. H., "A brief overview of solar and wind energy in Libya: Current trends and the future development", (2018).

49. Akroot, A., Almaktar, M., and Alasali, F., "The Integration of Renewable Energy into a Fossil Fuel Power Generation System in Oil-Producing Countries: A Case Study of an Integrated Solar Combined Cycle at the Sarir Power Plant", *Sustainability (Switzerland)* , 16 (11): (2024).

50. Ihbal, A., "Forecasting Short-Term Peak Load Demand in the Libyan Power Grid using Multiple Regression Model", *Journal Of Pure & Applied Sciences*, 22 (3): 124–128 (2023).

51. Abdunnabi, M. J. R. A., Dadesh, K. D. K., Mrehel, O. R. M. O. R., and El-shamekh, N. E. N., "Effect of full implementation of domestic solar water heaters on the electricity peak load in Libya", *Solar Energy And Sustainable Development Journal*, 5 (2): 33–43 (2016).

52. Ehtiwesh, I. A. S., Coelho, M. C., and Sousa, A. C. M., "Exergetic and environmental life cycle assessment analysis of concentrated solar power plants", *Renewable And Sustainable Energy Reviews*, 56: 145–155 (2016).

53. Tawil, I., Abeid, M., Abraheem, E., Alghoul, S., and Dekam, E., "Review on solar space heating-cooling in Libyan residential buildings", *Solar Energy And Sustainable Development Journal*, 7 (SI): 78–112 (2018).

54. Ehtiwesh, A., Kutlu, C., Su, Y., and Riffat, S., "Modelling and performance evaluation of a direct steam generation solar power system coupled with steam accumulator to meet electricity demands for a hospital under typical climate conditions in Libya", *Renewable Energy*, 206: 795–807 (2023).

55. Wang, M., Wang, J., Zhao, P., and Dai, Y., "Multi-objective optimization of a combined cooling, heating and power system driven by solar energy", *Energy Conversion And Management*, 89: 289–297 (2015).

56. Saini, P., Singh, J., and Sarkar, J., "Proposal and performance comparison of various solar-driven novel combined cooling, heating and power system topologies", *Energy Conversion And Management*, 205: 112342 (2020).

57. Chen, Y., Xu, J., Zhao, D., Wang, J., and Lund, P. D., "Exergo-economic assessment and sensitivity analysis of a solar-driven combined cooling, heating and power system with organic Rankine cycle and absorption heat pump", *Energy*, 230: 120717 (2021).

58. Wang, J., Dai, Y., Gao, L., and Ma, S., "A new combined cooling, heating and power system driven by solar energy", *Renewable Energy*, 34 (12): 2780–2788 (2009).

59. Cisek, P., Kaczmarski, K., Nowak-Ocłoń, M., Piwowarczyk, M., Ojczyk, G., and Vallati, A., "Design and performance calculations of a solar-driven combined cooling, heating and power system", *Energy*, 322: 135629 (2025).

60. Zhang, L., Li, F., Sun, B., and Zhang, C., "Integrated optimization design of combined cooling, heating, and power system coupled with solar and biomass energy", *Energies*, 12 (4): 687 (2019).

61. Liu, J., Li, Y., Meng, X., and Wu, J., "Thermodynamic analysis of a novel hybrid fuel cell-combined cooling, heating-and power (CCHP) system-integrated solar-driven biomass gasification for achieving sustainable and efficient poly-generation", *International Journal Of Green Energy*, 20 (13): 1524–1544 (2023).

62. Salimi, M., Hosseinpour, M., Mansouri, S., and N. Borhani, T., "Environmental aspects of the combined cooling, heating, and power (CCHP) systems: a review", *Processes*, 10 (4): 711 (2022).

63. Haghghi, M. A., Pesteei, S. M., Chitsaz, A., and Hosseinpour, J., "Thermodynamic investigation of a new combined cooling, heating, and power (CCHP) system driven by parabolic trough solar collectors (PTSCs): A case study", *Applied Thermal Engineering*, 163: 114329 (2019).

64. Saini, P., Singh, J., and Sarkar, J., "Thermodynamic, economic and environmental analyses of a novel solar energy driven small-scale combined cooling, heating and power system", *Energy Conversion And Management*, 226: 113542 (2020).

65. Wang, X., Duan, L., and Zheng, N., "Thermodynamic and economic analysis of a new CCHP system with active solar energy storage and decoupling of power and cooling outputs", *Energy*, 307: 132581 (2024).

66. Zhao, L., Zhang, Y., Deng, S., Ni, J., Xu, W., Ma, M., Lin, S., and Yu, Z., "Solar driven ORC-based CCHP: Comparative performance analysis between sequential and parallel system configurations", *Applied Thermal Engineering*, 131: 696–706 (2018).

67. Xia, H., Chen, J., Yuan, J., and Wang, Y., "Performance investigation and exergoeconomic optimization for a solar-driven direct heating and cooling system", *Journal Of Building Engineering*, 77: 107458 (2023).

68. Zarei, A., Akhavan, S., Rabiee, M. B., and Elahi, S., "Energy, exergy and economic analysis of a novel solar driven CCHP system powered by organic Rankine cycle and photovoltaic thermal collector", *Applied Thermal Engineering*, 194: 117091 (2021).

69. Li, Y., Wang, J., Zhou, Y., Wei, C., Guan, Z., and Chen, H., "Multi-dimension day-ahead scheduling optimization of a community-scale solar-driven CCHP system with demand-side management", *Renewable And Sustainable Energy Reviews*, 185: 113654 (2023).

70. Huang, Z. F., Chen, W. D., Wan, Y. D., Shao, Y. L., Islam, M. R., and Chua, K. J., "Techno-economic comparison of different energy storage configurations for renewable energy combined cooling heating and power system", *Applied Energy*, 356: 122340 (2024).

71. Nami, H., Anvari-Moghaddam, A., and Nemati, A., "Modeling and analysis of a solar boosted biomass-driven combined cooling, heating and power plant for

domestic applications", *Sustainable Energy Technologies And Assessments*, 47: 101326 (2021).

72. Behzadi, A. and Arabkoohsar, A., "Comparative performance assessment of a novel cogeneration solar-driven building energy system integrating with various district heating designs", *Energy Conversion And Management*, 220: 113101 (2020).

73. Borhani, S., Kasaeian, A., Pourmoghadam, P., and Omid, M., "Regional performance evaluation of solar combined cooling heating and power systems for household demands", *Applied Thermal Engineering*, 230: 120666 (2023).

74. Herrando, M., Pantaleo, A. M., Wang, K., and Markides, C. N., "Solar combined cooling, heating and power systems based on hybrid PVT, PV or solar-thermal collectors for building applications", *Renewable Energy*, 143: 637–647 (2019).

75. García-Domínguez, J., Blanco-Marigorta, A. M., and Daniel Marcos, J., "Analysis of a solar driven ORC-absorption based CCHP system from a novel exergy approach", *Energy Conversion And Management: X*, 19: 100402 (2023).

76. Chen, Y., Hua, H., Xu, J., Wang, J., Lund, P. D., Han, Y., and Cheng, T., "Energy, environmental-based cost, and solar share comparisons of a solar driven cooling and heating system with different types of building", *Applied Thermal Engineering*, 211: 118435 (2022).

77. Aieneh, K., Mehranfar, S., Yazdi Sotoude, M., Sadeghi, S., and Mahmoudzadeh Andwari, A., "Solar-Powered Combined Cooling, Heating, and Power Energy System with Phase-Change Material and Water Electrolysis: Thermo-Economic Assessment and Optimization", *Energies*, 17 (13): 3309 (2024).

78. Shakouri, A., Gorjian, S., and Ghobadian, B., "Energy, exergy, and exergoeconomic (3E) evaluation of a hybrid multigeneration system based on a solar tower", *Applied Thermal Engineering*, 252: (2024).

79. Alfaris, A., Akroot, A., Alqaed, S., and Almehmadi, F. A., "Performance analysis of integrated solar and natural gas combined cycle power plants in high solar potential regions", *Scientific Reports*, 15 (1): 9181 (2025).

80. Nourpour, M., Khoshgoftar Manesh, M. H., Pirozfar, A., and Delpisheh, M., "Exergy, Exergoeconomic, Exergoenvironmental, Emergy-based Assessment and Advanced Exergy-based Analysis of an Integrated Solar Combined Cycle Power Plant", *Energy And Environment*, 34 (2): 379–406 (2023).

81. Besevli, B., Kayabasi, E., Akroot, A., Talal, W., Alfaris, A., Assaf, Y. H., Nawaf, M. Y., Bdaiwi, M., and Khudhur, J., "Technoeconomic Analysis of Oxygen-Supported Combined Systems for Recovering Waste Heat in an Iron-Steel Facility", *Applied Sciences*, 14 (6): 2563 (2024).

82. Wang, J., Lu, Z., Li, M., Lior, N., and Li, W., "Energy, exergy, exergoeconomic and environmental (4E) analysis of a distributed generation solar-assisted

CCHP (combined cooling, heating and power) gas turbine system", *Energy*, 175: 1246–1258 (2019).

83. Talal, W. and Akroot, A., "An Exergoeconomic Evaluation of an Innovative Polygeneration System Using a Solar-Driven Rankine Cycle Integrated with the Al-Qayyara Gas Turbine Power Plant and the Absorption Refrigeration Cycle", *Machines*, 12 (2): 133 (2024).

84. Akroot, A. and Al Shammre, A. S., "Economic and Technical Assessing the Hybridization of Solar Combined Cycle System with Fossil Fuel and Rock Bed Thermal Energy Storage in Neom City", *Processes*, 12 (7): 1433 (2024).

85. Alfaris, A., Akroot, A., and Deniz, E., "The Exergo-Economic and Environmental Evaluation of a Hybrid Solar–Natural Gas Power System in Kirkuk", *Applied Sciences*, 14 (22): 10113 (2024).

86. Akroot, A., "Thermodynamic and Environmental Performance Analysis of the Marib Integrated Power and Cooling Cycle (MIPCC)", *Black Sea Journal Of Engineering And Science*, 8 (3): 814–823 .

87. Ren, J., Qian, Z., Yao, Z., Gan, N., and Zhang, Y., "Thermodynamic Evaluation of LiCl-H2O and LiBr-H2O Absorption Refrigeration Systems Based on a Novel Model and Algorithm", *Energies*, 12 (15): 3037 (2019).

RESUME

I am Salah Khalefa ABORAGIGA

I studied the Department of Mechanics in the city of Zintan and I study mechanical engineering at the University of Karabuk.